Geochemistry, Geophysics, Geosystems®

RESEARCH ARTICLE
10.1029/2024GC011750

Identifying Recycled Materials Using Mo Isotopes in Intraplate Alkali Basalts From the Southeastern Margin of Tibetan Plateau

Dongjing Xu[1,2], Yue Qi[1], Qiang Wang[1,2], Jie Li[1], Derek A. Wyman[3], Andrew C. Kerr[4], Xiuzheng Zhang[1], and Peina Guo[1,2]

[1]State Key Laboratory of Isotope Geochemistry, Guangzhou Institute of Geochemistry, Chinese Academy of Sciences, Guangzhou, China, [2]College of Earth and Planetary Sciences, University of Chinese Academy of Sciences, Beijing, China, [3]School of Geosciences, The University of Sydney, Sydney, NSW, Australia, [4]School of Earth and Environmental Sciences, Cardiff University, Cardiff, UK

Key Points:

- Miocene Maguan basalts have similar Sr-Nd-Pb isotopic compositions but a large range of Mo isotopic compositions
- Recycled serpentinized peridotites yield high $\delta^{98/95}$Mo values, while recycled oceanic crust and sediments yield low $\delta^{98/95}$Mo values
- Mo isotopes are effective tools to trace complex slab fluxes generating mantle geochemical heterogeneity

Supporting Information:

Supporting Information may be found in the online version of this article.

Correspondence to:

Y. Qi and Q. Wang,
qiyue2233@163.com;
wqiang@gig.ac.cn

Citation:

Xu, D., Qi, Y., Wang, Q., Li, J., Wyman, D. A., Kerr, A. C., et al. (2024). Identifying recycled materials using Mo isotopes in intraplate alkali basalts from the southeastern margin of Tibetan Plateau. *Geochemistry, Geophysics, Geosystems*, *25*, e2024GC011750. https://doi.org/10.1029/2024GC011750

Received 10 JUL 2024
Accepted 10 OCT 2024

Author Contributions:

Conceptualization: Yue Qi
Data curation: Dongjing Xu, Yue Qi
Formal analysis: Dongjing Xu, Yue Qi
Funding acquisition: Qiang Wang
Investigation: Dongjing Xu, Yue Qi, Qiang Wang, Xiuzheng Zhang, Peina Guo
Methodology: Jie Li
Project administration: Qiang Wang
Supervision: Qiang Wang
Visualization: Dongjing Xu
Writing – original draft: Dongjing Xu

Abstract Mantle heterogeneity in lithology and geochemistry is often attributed to recycled subducted materials. While distinct mantle end-members are identified by radiogenic isotopes, the specific recycled materials contributing to this heterogeneity remain debated. This study presents Mo-Sr-Nd-Pb isotopic data for OIB-like alkali basalts from the Maguan area in the southeastern Tibetan Plateau, focusing on slab inputs' role in mantle heterogeneity. The Miocene (ca. 13 Ma) Maguan alkali basalts are divided into two types based on petrographic and geochemical characteristics, showing similar Sr-Nd-Pb isotopic signatures but different Mo isotopic compositions. Type I basalts exhibit a wide $\delta^{98/95}$Mo range (−0.31‰ to −1.03‰, average −0.47‰ ± 0.06‰, 2SD = 0.40‰, n = 13), while type II basalts have heavy and constant $\delta^{98/95}$Mo values (−0.11‰ to −0.17‰, average −0.14‰ ± 0.01‰, 2SD = 0.05‰, n = 6). The unique low $\delta^{98/95}$Mo value (−1.03‰) in type I basalts is among the lowest reported in OIB-like continental basalts. Type I basalts likely originate from an enriched asthenospheric mantle metasomatized by melts from recycled dehydrated oceanic crust and sediments, whereas type II basalts are derived from partial melting of an enriched asthenospheric mantle metasomatized by melts from recycled serpentinized peridotites. The residual Tethys oceanic slabs in the deep mantle significantly contribute to the mantle source of the Maguan basalts. The formation of Maguan Miocene magmas may be linked to mantle upwelling induced by the subduction of the West Burma plate. This study highlights the Mo isotopic system's utility in tracing complex slab fluxes generating mantle geochemical heterogeneity.

Plain Language Summary Recycling of subducted material can exert a profound influence on the deep mantle. Tracing superficial substances in the mantle is crucial for understanding Earth's evolution. However, radiogenic isotopic compositions for different enriched mantle end-members overlap, hindering our understanding of which specific recycled materials contribute to enriched mantle end-members. In this paper, we solve this problem by studying the molybdenum (Mo) isotope system in Cenozoic mantle-derived basalts from the southeastern margin of the Tibetan Plateau. Our findings show that although the studied basalts have similar ratios of radiogenic isotopes, they can be divided into two types based on petrographic and geochemical characteristics, especially Mo isotopes. We attribute recycled dehydrated oceanic crust with sediments to isotopically lighter Mo and serpentinized peridotites to isotopically heavier Mo in their mantle sources. This study shows the mantle heterogeneity for Mo isotopes, and in turn demonstrates that the Mo isotope system for mantle-derived magmas is an effective tool to track substances in the Earth's interior.

1. Introduction

Recycling of crustal materials results in variable geochemical and lithological enrichment in the deep mantle and is crucial for understanding Earth's evolution (Eriksen & Jacobsen, 2022; Gamal El Dien et al., 2020). Although over the last 50 years or so there has been a significant amount of research into which subducted crustal materials contribute to enriched mantle, the issue is still controversial (Elliott et al., 2006; Hofmann, 1997; Jackson et al., 2007; Ma et al., 2022). Our understanding of enriched mantle is mainly based on the trace elements and isotopic compositions of mantle-derived melts, such as oceanic island basalts (OIBs) (Doucet et al., 2020; Hofmann, 1997; S. S. Sun & McDonough, 1989; Weaver, 1991) and continental basalts (Z.-Z. Wang et al., 2018; H.-F. Zhang et al., 2003). According to their radiogenic isotopic (e.g., Sr-Nd-Pb-Hf) compositions, a range of

Writing – review & editing: Yue Qi, Qiang Wang, Derek A. Wyman, Andrew C. Kerr

typical enriched "end-member" mantle components have been identified, including HIMU (high $^{238}U/^{204}Pb$), EM1 (enriched mantle 1) and EM2 (enriched mantle 2) (e.g., Zindler & Hart, 1986). However, radiogenic isotopic compositions for most OIBs and continental basalts have intermediate compositions between these enriched mantle end-members (e.g., Lei et al., 2021; Wagner et al., 2023). As a result, it is difficult to identify the specific contributions of various recycled materials to these mantle end-members from radiogenic isotopes alone.

The rapid development of multi-collector inductively coupled plasma mass spectrometry (MC-ICP-MS) has elevated the utility of stable isotope systematics, making them invaluable geochemical tools that complement radiogenic isotopes in investigating mantle heterogeneity (Eriksen & Jacobsen, 2022; Teng et al., 2017). Thus, a combination of stable isotopes and radiogenic isotopes can be used to provide new perspectives on recycled materials (Ma et al., 2022; Tian et al., 2016; Wagner et al., 2023). An ideal tool to probe mantle heterogeneity should feature significant variations across different reservoirs, exert a significant impact on the compositions of the mantle, and remain largely resistant to perturbations en route back to the surface. While Mo (Molybdenum) isotopes can be affected by crustal contamination due to their incompatible behavior, careful selection of samples and geochemical screening can minimize these effects, making Mo isotopes powerful tracers for slab recycling (Willbold & Elliott, 2017).

Mo is a highly incompatible element with a bulk distribution coefficient comparable to that of light rare earth elements (LREEs) and thus concentrates in melts during mantle melting (Liang et al., 2017). On this basis, Mo abundances in the continental and oceanic crust are much higher than in the putative primitive mantle or the depleted mantle (DM). According to estimates based on mid-ocean ridge basalts (MORBs) (Bezard et al., 2016; Chen et al., 2022; Hin et al., 2022), komatiites, picrites (McCoy-West et al., 2019), and mantle xenoliths (Liang et al., 2017), the $\delta^{98/95}$Mo value of the Earth's mantle is around −0.20‰ (McCoy-West et al., 2019). Sediments, including black shales ($\delta^{98/95}$Mo = 0‰ to +1.7‰; Freymuth et al., 2016; L. Xu et al., 2012) and marine carbonates (mean $\delta^{98/95}$Mo = +1.43 ± 0.97‰, mean Ce/Mo = 1.43, Y. Zhang et al., 2020 and references therein), generally exhibit heavy Mo isotope signatures. A significant proportion of sediments, however, show isotopically light Mo with $\delta^{98/95}$Mo values extending to −1.87‰ (Freymuth et al., 2015). Oceanic MORB-type eclogites, representing recycled oceanic crust, also possess isotopically light Mo ($\delta^{98/95}$Mo = −0.68 to −0.13‰, Chen et al., 2019). The large Mo concentration and Mo isotopic compositional variation among different terrestrial reservoirs suggest that Mo isotopes can be sensitive tracers for crustal material recycling (Kendall et al., 2017).

In this study, we report the major and trace elements and Sr-Nd-Pb-Mo isotopic compositions of the Miocene (ca. 13 Ma) Maguan alkali basalts in the southeastern Tibetan Plateau. The alkali basalts contain mantle xenoliths, and display OIB-like trace element patterns, indicating that they ascended rapidly without suffering significant crustal assimilation and crystallization (Lei et al., 2021; C.-Z. Liu et al., 2013; S.-A. Liu et al., 2020; Spera, 1984). The Maguan basalts can be classified into two types based on petrographic features and whole-rock compositions. These two types show similar Sr-Nd-Pb isotopic compositions but distinct Mo isotopic compositions. Our study demonstrates that Mo isotope system provide an efficient way to distinguish between different subducted components that can contribute to mantle enrichment.

2. Geological Setting and Sample Description

The Ailaoshan-Red River shear zone (ARSZ), situated at the southeastern margin of the Tibetan Plateau, is a significant tectonic boundary between the Yangtze Craton to the east and the Indochina Block to the west (Figure 1a; X. Wang et al., 2000). The India-Asia continental collision triggered significant sinistral slip on the ARSZ (Gilley et al., 2003), triggering the movement of the Indochina Block toward the southeast by ∼500–700 km (Chung et al., 1997; Tapponnier et al., 1982). Seismic observations have revealed that subducted Neo-Tethys Oceanic slab may reside in the mantle transition zone (MTZ) beneath the ARSZ and the area has experienced a relatively stable intraplate setting since closure of the Neo-Tethys Ocean at least before 45 Ma (J. Huang & Zhao, 2006; Ji et al., 2016; C. Li et al., 2008; M. Xu et al., 2018). Two distinct Cenozoic episodes of mafic magmatism have been identified along the ARSZ, occurring either before or after the left-lateral movement along this significant fault. The first is found in the Dali-Lijiang area and neighboring regions of western Yunnan and Sichuan and was related to a period of potassic to ultrapotassic activity, spanning the Late Eocene to the Early Oligocene (Flower et al., 2013; Guo et al., 2005; X.-L. Huang et al., 2010; J.-H. Wang et al., 2001). The second, younger episode of magmatism, which occurred in the Pliocene or earlier in the Pleistocene, includes basalt and basanite phases with high sodium content (Flower et al., 2013; X.-K. Huang et al., 2013; Lei et al., 2021; S.-A. Liu

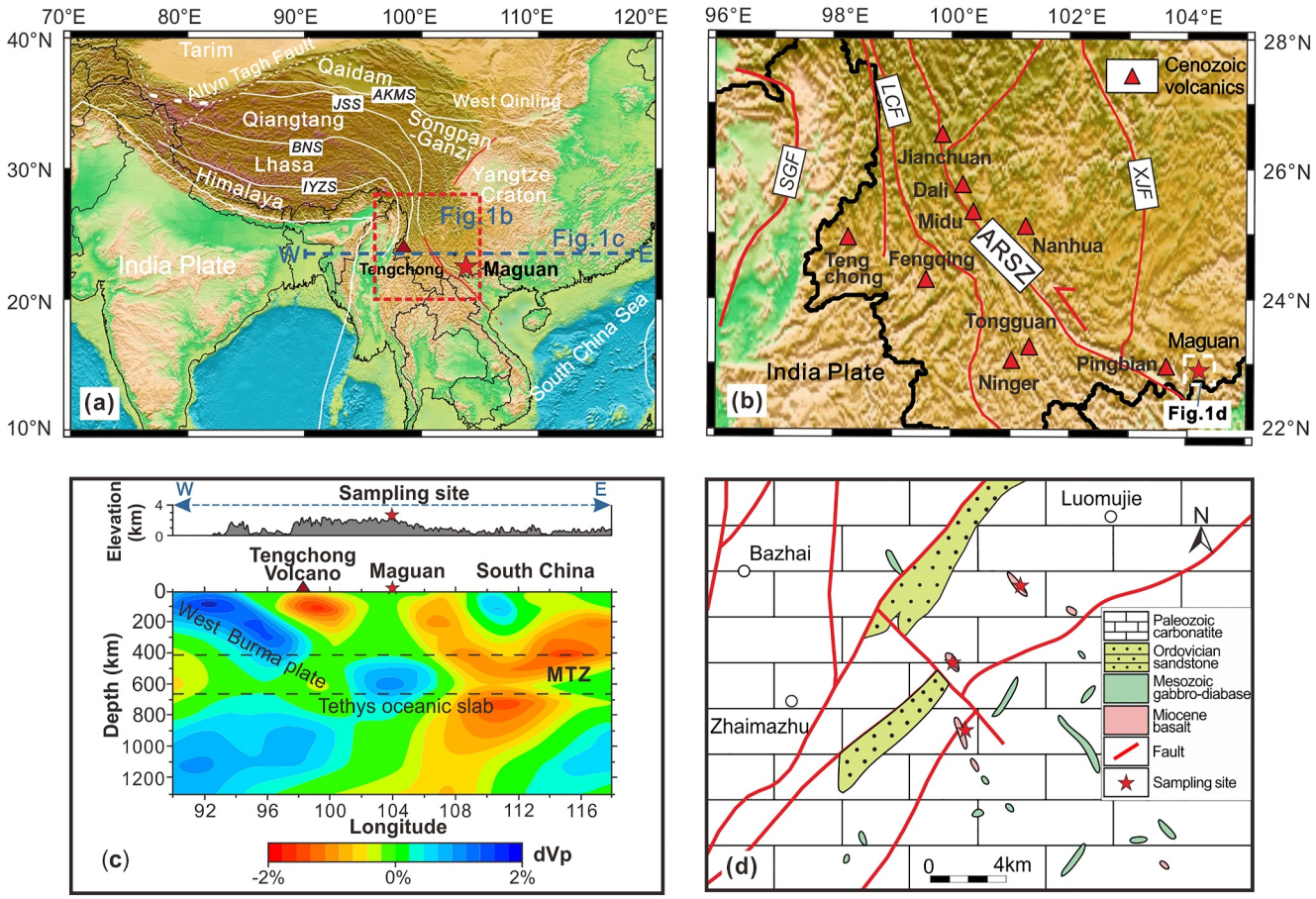

Figure 1. (a) Map of the Tibetan plateau and its surroundings with major geological blocks and plate boundaries. The dashed blue line (W–E) is the profile shown in panel (c). (b) Topography of study area and its surrounding regions and the distribution of Cenozoic volcanics (X.-K. Huang, 2012; X.-L. Huang et al., 2010; Lei et al., 2021; J.-H. Wang et al., 2001). SGF, Sagaing Fault; LCF, Lancangjiang Fault; XJF, Xiaojiang Fault; (c) Surface topography (top) and vertical cross-section P-wave tomography (bottom) along the profile (W–E) shown in panel (a) (J. Huang & Zhao, 2006). (d) Geological map of the Maguan region and sample locations.

et al., 2020; Xia & Xu, 2006). This study focuses on Cenozoic basalts from Maguan, Yunnan, which are part of the younger episodes of magmatism.

The studied outcrops of Maguan alkali basalts occur as explosive breccia and intruded the Cambrian-Ordovician strata during the Miocene (12.2–11.6 Ma, biotite $^{40}Ar/^{39}Ar$ ages, J.-H. Wang et al., 2001; 13.3–11.7 Ma, groundmass $^{40}Ar/^{39}Ar$ ages X.-K. Huang, 2012) and cover around 8 km^2 close to a series of N-S-trending rifts (Figure 1d; Lei et al., 2021). Twenty-five samples of basalt with no significant sign of alteration were collected. Samples are divided into two types based on petrographic observation. The type I basalts show typical porphyritic textures with subhedral-euhedral phenocrysts composed of 3%–5% olivine (0.1–0.4 mm), 3%–6% clinopyroxene (<0.2 mm) and 2%–4% plagioclase (<0.2 mm) set in a fine-grained groundmass mainly of plagioclase, K-feldspar, albite, clinopyroxene and olivine (Figure 2c). Type II basalts also have porphyritic textures but contain dominant olivine phenocrysts (0.1–0.4 mm, 4%–6%) and accessory clinopyroxene phenocrysts. Their groundmasses contain less plagioclase or albite but more clinopyroxene, K-feldspar and glass compared to those of type I basalts (Figure 2d).

3. Results

The analytical methods and data are provided in Supporting Information S1. $^{40}Ar/^{39}Ar$ analyzed on the groundmass of whole rocks are shown in Table S1 and in Figure S1 in Supporting Information S1. Whole-rock major and trace elements as well as Sr-Nd-Pb isotopic compositions are shown in Table S2 and Table S3 in Supporting Information S1. Major elements in olivine are shown in Table S4 in Supporting Information S1.

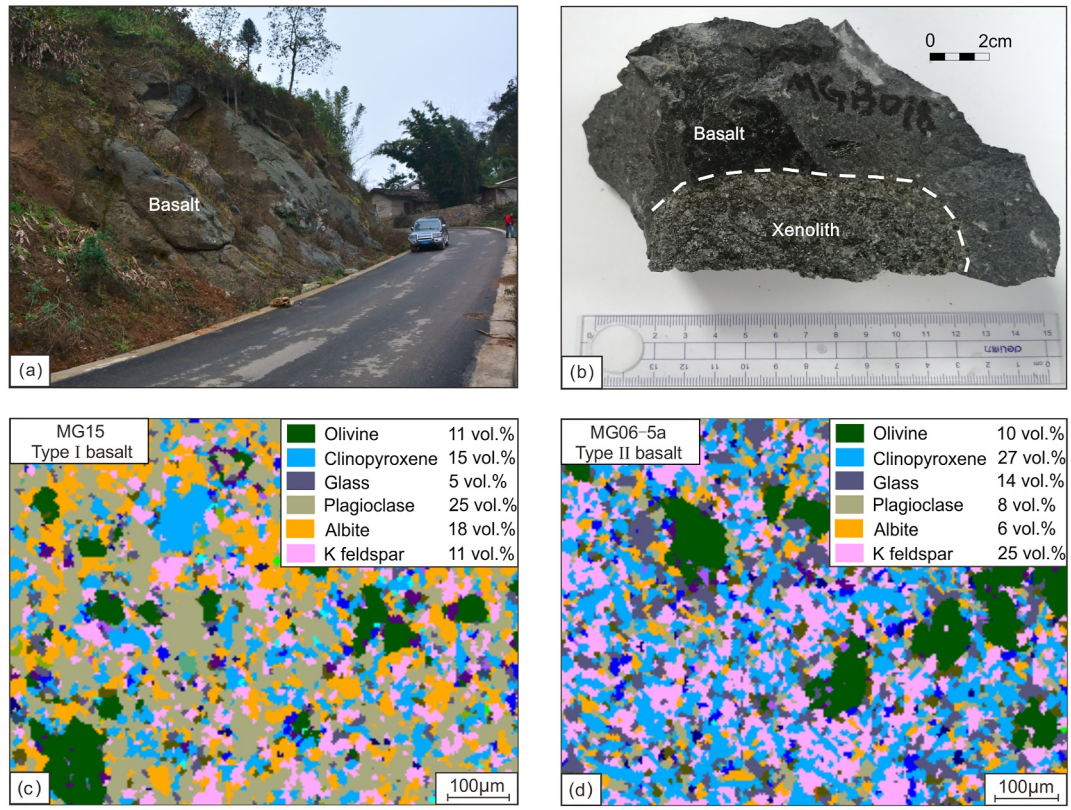

Figure 2. (a) Outcrop photograph of basalt in the Magun region. (b) Photograph of a basalt hand specimen containing mantle xenoliths. (c) TIMA image of representative Maguan type I basalt. (d) TIMA image of representative Maguan type II basalt.

Molybdenum concentrations and $\delta^{98/95}$Mo data obtained in this study as well as age-corrected Sr-Nd-Pb isotopic data are presented in Table 1.

3.1. ^{40}Ar-^{39}Ar Dating

The ^{40}Ar-^{39}Ar dating based on groundmass yielded concordant age spectra with plateau ages of 11.02 ± 0.23 Ma (2SE, $\Sigma^{39}Ar_k$ = 54.10%, Figure S1a in Supporting Information S1) and 13.16 ± 0.18 Ma (2SE, $\Sigma^{39}Ar_k$ = 100%, Figure S1b in Supporting Information S1) for the type I basalts and 12.49 ± 0.14 Ma (2SE, $\Sigma^{39}Ar_k$ = 95.23%, Figure S1c in Supporting Information S1) for the type II basalts. The inverse isochron ages are consistent with the plateau ages (Figure S1 in Supporting Information S1). Our ^{40}Ar-^{39}Ar dating results indicate that the two types of Maguan basalts erupted within the same Miocene time window, in line with the ^{40}Ar-^{39}Ar age (11.9 ± 0.3 Ma) from biotite of the related basaltic trachy-andesite reported by J.-H. Wang et al. (2001) and basalt groundmass ^{40}Ar-^{39}Ar age (13.3–11.7 Ma) reported by X.-K. Huang (2012).

3.2. Elemental Compositions of Whole Rocks and Olivines

Most of the type I basalts are trachy-basalts, with a minor occurrence of basanites (Figure 3a), based on the TAS (Total Alkali-Silica) classification scheme of Le Bas et al. (1986). They have SiO_2 contents of 46.1–48.3 wt.%, CaO contents of 7.0–8.4 wt. %, and MgO contents of 8.0–10.7 wt.% (Figure 3b; Table S2 in Supporting Information S1). On a CaO-Zn/Fe*10000 whole rock plot and the Ni-1000Mn/Fe plot for olivine, most type I samples plot in the field of pyroxenite melt influence (Figures 3b and 3c). Type I basalts are enriched in LREEs with no negative Eu anomalies (Figure 4). On a primitive mantle-normalized diagram, all samples exhibit significant enrichment in large-ion lithophile elements (LILEs) and positive Nb, Ta, Pb, Zr anomalies with slight negative anomalies of Ti and Y (Figure 4b). Type II basalts are all basanites, based on the TAS classification scheme, and have lower SiO_2 contents (43.1–44.7 wt. %) than type I basalts. They have higher MgO (8.9–10.8 wt. %) and CaO (8.4–9.2 wt. %) contents than type I basalts (Figure 3b; Table S2 in Supporting Information S1). On a CaO-Zn/

Table 1
Mo Isotope, Mo Concentration, and Corresponding Sr-Nd-Pb Isotope Data for Maguan Alkali Basalts

Sample	Rock type	$\delta^{98/95}$Mo (‰)	2SE	Mo (μg/g)	Ce/Mo	$^{87}Sr/^{86}Sr_i$	$^{143}Nd/^{144}Nd_i$	$\varepsilon_{Nd}(t)$	$^{206}Pb/^{204}Pb_i$	$^{207}Pb/^{204}Pb_i$	$^{208}Pb/^{204}Pb_i$
MG03-5	Type I basalts	−0.72	0.04	2.76	17.87	0.704376	0.512904	5.47	18.3803	15.5969	38.6550
MG08-3	Type I basalts	−0.31	0.04	3.06	14.24	0.703773	0.512964	6.67	18.5709	15.6137	38.6584
MG08-4	Type I basalts	−0.41	0.04	2.86	17.94						
MG08-6-2	Type I basalts	−0.32	0.04	3.12	17.26						
MG04	Type I basalts	−0.50	0.06	2.97	16.02	0.704234	0.512935	6.10	18.3857	15.5533	38.4222
MG05	Type I basalts	−0.36	0.05	3.26	14.74	0.704356	0.512932	6.04	18.8142	15.6751	39.1191
MG06	Type I basalts	−0.45	0.02	2.88	16.05						
MG06 R	Type I basalts	−0.43	0.02	3.18	16.24						
MG09	Type I basalts	−0.43	0.06	2.67	18.48						
MG10	Type I basalts	−0.36	0.04	2.63	18.77	0.704186	0.512913	5.68	18.4661	15.5943	38.5939
MG11	Type I basalts	−1.03	0.05	3.24	14.57	0.704588	0.512909	5.56	18.3701	15.5972	38.6510
MG13	Type I basalts	−0.44	0.06	3.25	15.09						
MG15	Type I basalts	−0.33	0.04	3.25	14.70	0.704330	0.512924	5.86	18.4104	15.5613	38.4328
MG06-2	Type II basalts	−0.15	0.03	5.54	14.37						
MG06-3	Type II basalts	−0.17	0.03	6.07	13.17	0.703771	0.512980	6.95	18.1290	15.4785	37.9876
MG06-5	Type II basalts	−0.12	0.04	6.17	13.72	0.703791	0.512981	6.97	18.1286	15.4777	37.9863
MG06-5R	Type II basalts	−0.16	0.03	6.24	11.70						
MG01	Type II basalts	−0.14	0.05	5.94	13.39						
MG02	Type II basalts	−0.11	0.02	6.26	11.95						

Standards	References	$\delta^{98/95}$Mo (‰)	2SE	Mo (μg/g)	*n*
NIST3134	This study	0.00	0.07		20
IAPSO-seawater	This study	2.07	0.07	0.01	3
IAPSO-seawater	Zhao et al. (2016)	2.02	0.06	0.01	20
AGV-2	This study	−0.15	0.05	1.96	2
AGV-2	Willbold et al. (2016)	−0.15	0.05	1.96	3
GSR-3	This study	−0.47	0.07	3.00	2
GSR-3	Zhao et al. (2016)	−0.51	0.04	2.92	1

Note. R: sample replicate.

Fe*10000 plot for whole rock and Ni-100Mn/Fe plot for olivine, most type II samples plot in the peridotite melt field (Figures 3b and 3c). They are enriched in LREEs and LILEs with positive Nb, Ta, Zr anomalies and slight negative anomalies of Ti and Hf (Figure 4). The absence of positive Pb anomaly distinguishes type II basalts from type I basalts.

3.3. Sr-Nd-Pb Isotopes of Whole Rocks

Initial Sr, Nd, and Pb isotopes were calculated at $t = 12$ Ma. Type I basalts have $(^{87}Sr/^{86}Sr)_i$ values of 0.703773–0.704588 and $\varepsilon_{Nd}(t)$ values of 5.47–6.67 (Table S3 in Supporting Information S1; Figure 5c). Their $^{206}Pb/^{204}Pb_i$, $^{207}Pb/^{204}Pb_i$ and $^{208}Pb/^{204}Pb_i$ ratios are 18.370 to 18.814, 15.553 to 15.675, 38.422 to 39.119, respectively (Figures 5b and 5d). Although the two types of basalts show similar Sr-Nd-Pb isotopic compositions, type II basalts have slightly more depleted Sr-Nd isotopic compositions than type I samples. They have $(^{87}Sr/^{86}Sr)_i$ values of 0.703771 and 0.703791, $\varepsilon_{Nd}(t)$ values of 6.9–7.0 (Table S3 in Supporting Information S1; Figure 5c). They display $^{206}Pb/^{204}Pb_i$, $^{207}Pb/^{204}Pb_i$ and $^{208}Pb/^{204}Pb_i$ ratios of 18.129, 15.478, 37.986 to 37.988, respectively (Figures 5b and 5d). Generally, the isotopic ratios of Nd and Sr in both types of basalts lie in or close to the DM field (Figure 5c), thus implying an asthenospheric origin. The Pb isotopic compositions clearly reflect a hybrid of EM1 and DM mantle sources (Figures 5b and 5d).

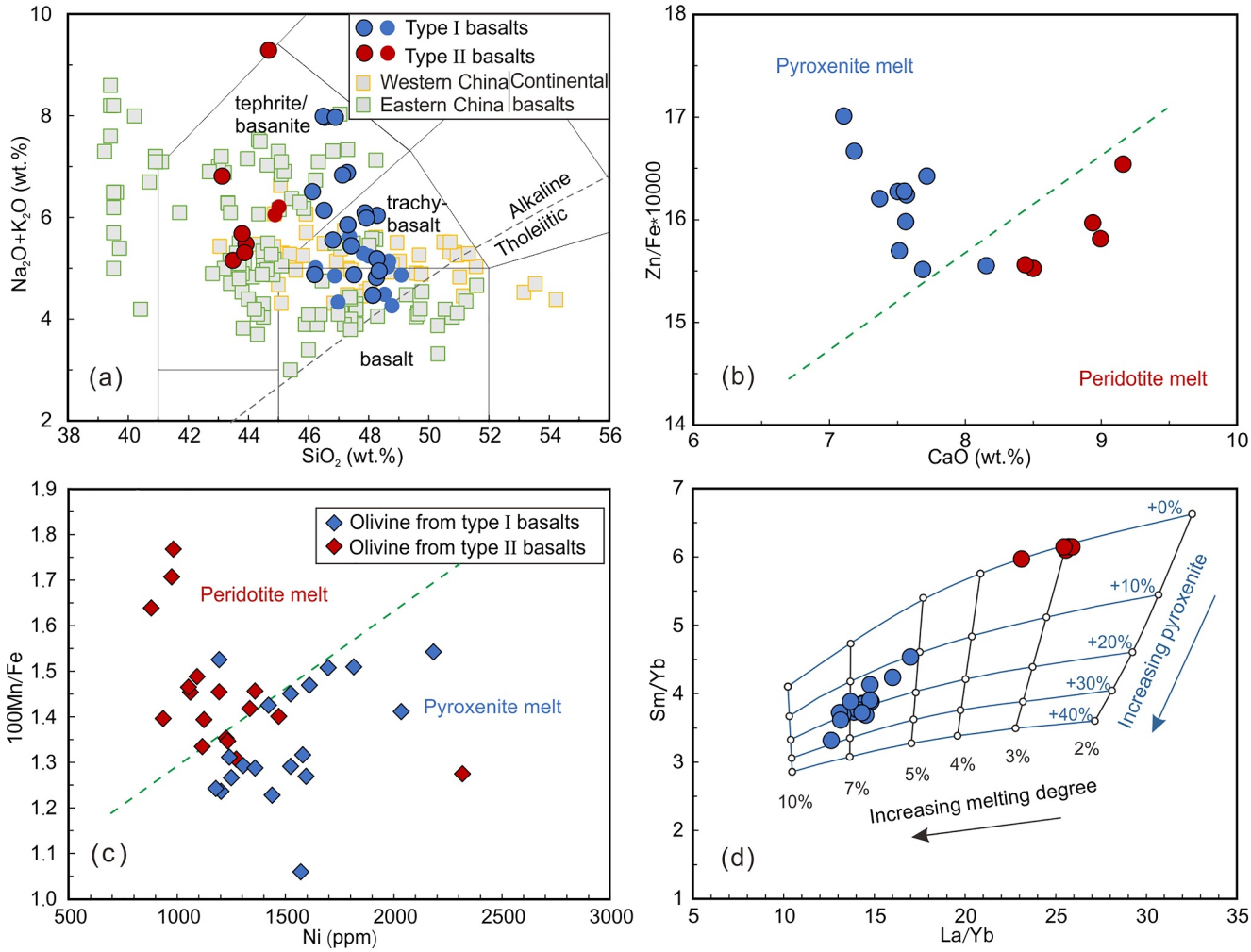

Figure 3. (a) SiO_2 (wt.%) versus total alkali diagram classifying alkali lava from Maguan, southeastern Yunna, along with literature data (Lei et al., 2021; S.-A. Liu et al., 2020) and data for continental intraplate basalts from western China (Cheng et al., 2022; Xie et al., 2023) and eastern China (Z.-Z. Wang & Liu, 2021; Z.-Z. Wang et al., 2018; Zou et al., 2022). (b) CaO (wt.%) versus Zn/Fe ($\times 10^4$) of Maguan basalts. The green dashed line is the trend discriminating mantle sources dominated by peridotites or pyroxenites referenced by Bowman and Ducea (2023). (c) Ni (ppm) versus Mn/Fe ($\times 10^2$) of olivine from Maguan basalts. (d) La/Yb versus Sm/Yb diagram for Maguan basalts. Also shown is a partial melting model of a hypothetical mantle source consisting of peridotites and garnet pyroxenites. The peridotite is assumed to be composed of 60% olivine, 15% clinopyroxene, 10% garnet, and 15% orthopyroxene, while the garnet pyroxenite consists of 90% clinopyroxene and 10% garnet in mineralogy, as proposed by Cheng et al. (2022). The elemental abundances are from McDonough and Sun (1995), and the partition coefficients are from Rollinson (1993) as follows: La: olivine = 0.0067, clinopyroxene = 0.03, garnet = 0.001, orthopyroxene = 0.047; Sm: olivine = 0.028, clinopyroxene = 0.30, garnet = 0.02, orthopyroxene = 0.1; Yb: olivine = 0.014, clinopyroxene = 0.40, garnet = 5.0, orthopyroxene = 0.049. The black numbers represent degrees of partial melting, while the blue numbers represent proportions of garnet pyroxenites.

3.4. Whole Rock Mo Isotope Compositions

Type I basalts have Mo concentrations of 2.63–3.26 ppm, which are higher than MORB (0.07–1.93 ppm, Bezard et al., 2016; Chen et al., 2022), bulk continental crust (0.8 ppm, Rudnick & Gao, 2014), and arc lava (0.4–1.3 ppm, Freymuth et al., 2015) but are similar to OIBs (0.7–4.2 ppm, Liang et al., 2017). The Ce/Mo ratios of type I basalts vary from 14 to 19 (Table 1), which is higher than the normal mantle value of approximately 0.03 (Newsom et al., 1986). The $\delta^{98/95}$Mo values of type I basalts show a large range of −0.31‰ to −1.03‰ (mean −0.47‰, n = 13, Table 1), which are significantly lower than those of MORBs and global mantle xenoliths. Some of the values ranging from −0.50‰ to −0.31‰ are similar to Mediterranean lamproites, subduction-related igneous rocks, and MORB-type eclogites (−0.68‰ to −0.13‰; Figure 6; Chen et al., 2019), while two samples show much lower $\delta^{98/95}$Mo values (−1.03‰ and −0.72‰) than those of reported oceanic eclogites. The type II basalts exhibit higher Mo concentrations (5.5–6.3 ppm) and lower Ce/Mo ratios (12–14) than those of the type I basalts. The $\delta^{98/95}$Mo values of the type II basalts are −0.11‰ to −0.17‰, with an average of −0.14‰ (n = 6), which is

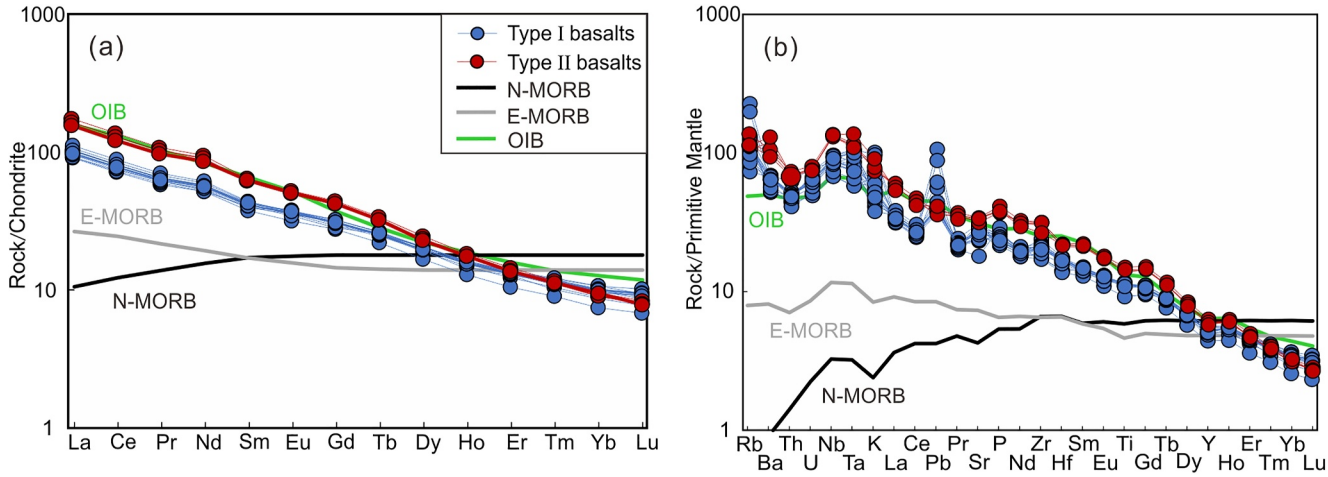

Figure 4. Diagrams of (a) Chondrite-normalized (S. S. Sun & McDonough, 1989) rare earth element patterns of Maguan alkali basalts and (b) trace element patterns of Maguan alkali basalts normalized to primitive mantle values (S. S. Sun & McDonough, 1989). The comparison plots of oceanic island basalt, E-MORB and N-MORB are all from S. S. Sun and McDonough (1989).

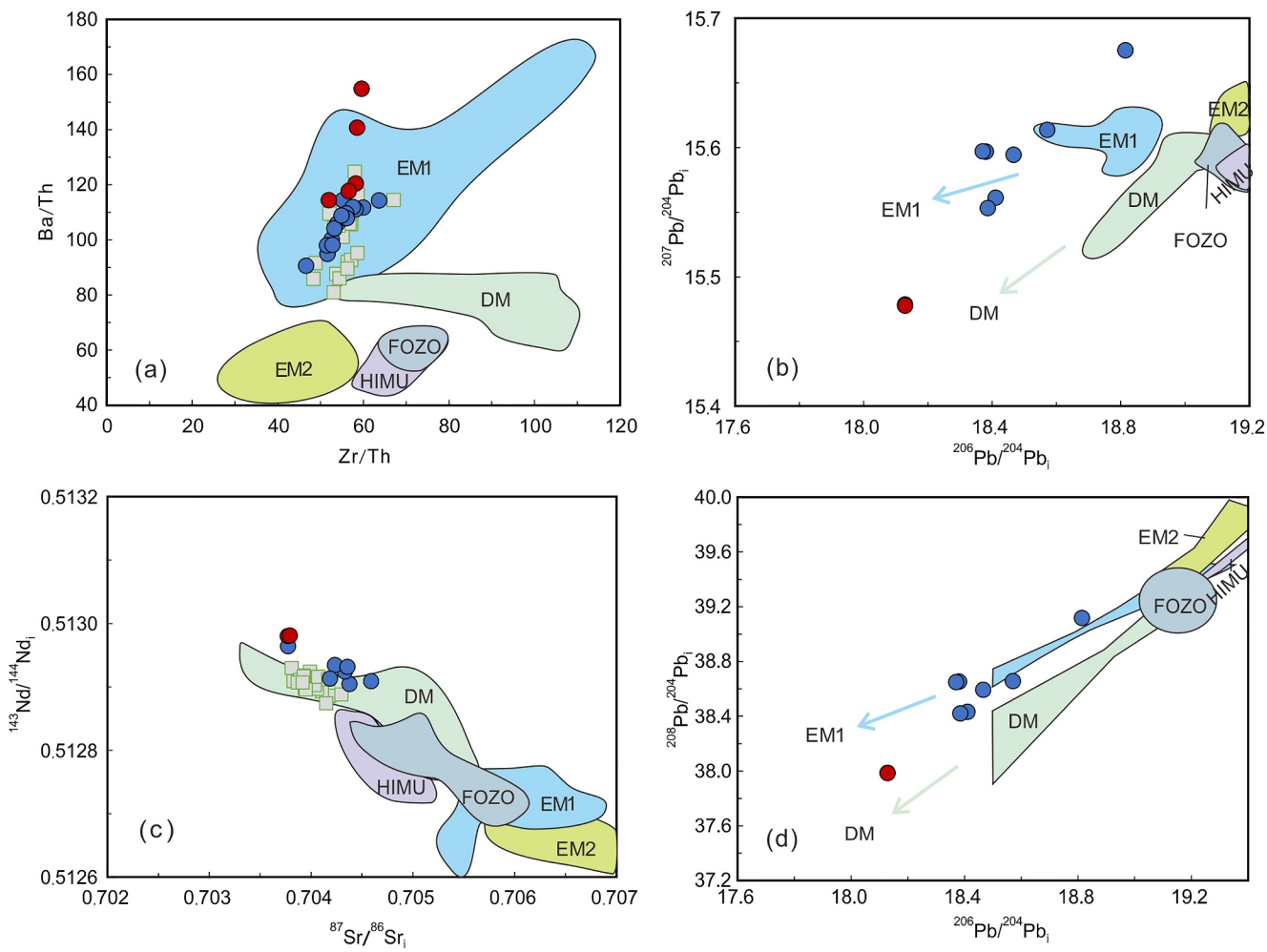

Figure 5. Diagrams of (a) Zr/Th versus Ba/Th; (b) $^{206}Pb/^{204}Pb_i$ versus $^{207}Pb/^{204}Pb_i$; (c) $^{87}Sr/^{86}Sr_i$ versus $^{143}Nd/^{144}Nd_i$; (d) $^{206}Pb/^{204}Pb_i$ versus $^{208}Pb/^{204}Pb_i$ for Maguan alkali basalts. Data sources for the DM, HIMU, EM1, EM2 fileds are from Reinhard et al. (2019) and Jackson et al. (2014). Data for Cenozoic intraplate alkali basalts from eastern China represented by gray rectangles with a green border are from Zou et al. (2022).

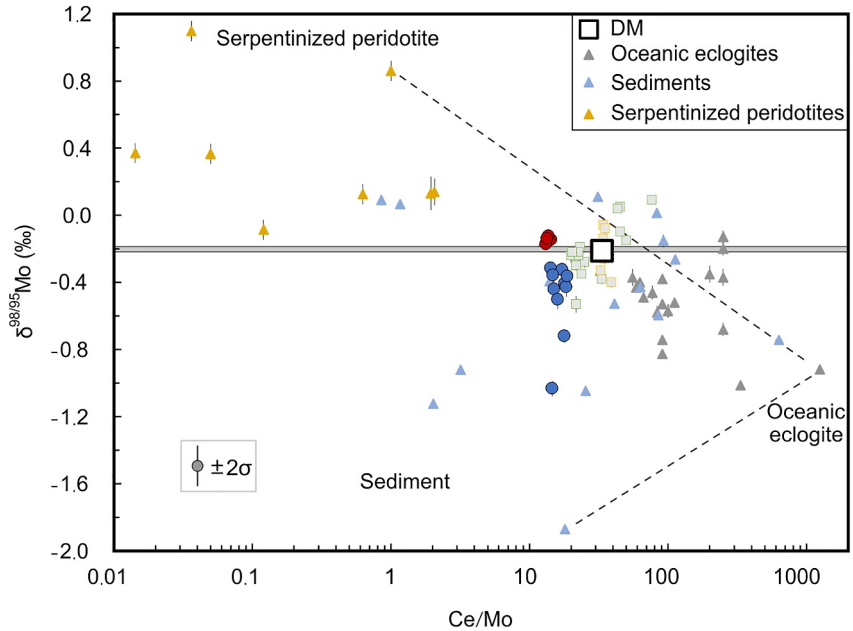

Figure 6. Diagram of Ce/Mo (log-scale) versus $\delta^{98/95}$Mo (‰) for Maguan alkali basalts. Ce/Mo ratio and $\delta^{98/95}$Mo of DM are 33.4 (Gale et al., 2013) and −0.20‰ (Bezard et al., 2016; McCoy-West et al., 2019), respectively. Data for oceanic eclogites representing subducted oceanic crust are from Chen et al. (2019) and Ahmad et al. (2021). Data for sediments are from Freymuth et al. (2015). Data for serpentinized peridotites are from Chen et al. (2019) and Rojas-Kolomiets et al. (2023). Data for continental alkali basalts from western China and eastern China are from Y. Zhang et al. (2019) and Fang, Dai, Zheng, and Zhao (2023), respectively.

slightly higher than those of the Earth's mantle represented by MORBs (−0.206 ± 0.02‰, Bezard et al., 2016) and global mantle xenoliths (−0.206 ± 0.05‰, Liang et al., 2017).

4. Discussion

4.1. Contrasting Mo Isotopic Variations of the Mantle Source

All studied Maguan alkali basalts contain mantle xenoliths (Figure 2b), indicating that they ascended rapidly to the surface from the mantle source (Lei et al., 2021; C.-Z. Liu et al., 2013; S.-A. Liu et al., 2020; Spera, 1984). This implies that crustal contamination and fractional crystallization did not significantly affect their geochemical compositions. This inference is also supported by high Nb/U (mean 47.3 for type I basalts and mean 59.2 for type II basalts) and Nb/La (mean 2.6 for type I basalts and mean 2.4 for type II basalts) ratios and no correlation between MgO contents and Sr-Nd-Pb-Mo isotopic values (Figure S2 in Supporting Information S1). Despite the fact that the LOI (Loss on Ignition) values indicate that the samples have undergone minor alteration, the lack of correlation between LOI values and Mo isotopic values suggests that low-temperature alteration has little effect on the Mo isotopic composition of the samples (Figure 7a). The good correlations between the fluid-immobile Nb and fluid-mobile elements (e.g., Th, U; Figure S3 in Supporting Information S1) also suggest low-temperature alteration effects were insignificant. We therefore argue that all studied Maguan alkali basalts are strong candidates for being primary or near-primary magma.

The two types of Maguan alkali basalts display similar trace element patterns and Sr-Nd-Pb isotopic compositions (Figures 4 and 5b–5d), but they contrast strongly in terms of Mo isotopic compositions (Figures 6–8). As discussed above, we have excluded the possibility that the Mo isotopic variation is caused by crustal contamination and the fractional crystallization processes. Some studies have suggested that fractional crystallization of TiO_2-rich minerals can lead to Mo isotope fractionation (e.g., L. Zhang et al., 2024). Specifically, 50% fractional crystallization of Fe-Ti oxides (e.g., magnetite and ilmenite) can result in a 0.15‰ shift in $\delta^{98/95}$Mo under QFM conditions (L. Zhang et al., 2024). In our samples, the TiO_2 content ranges narrowly from 2.29 wt.% to 3.26 wt.% (Figure 7c), indicating that the extent of fractional crystallization of TiO_2-rich minerals is very limited and far from reaching 50%. This degree of crystallization is insufficient to cause such significant Mo isotope variation

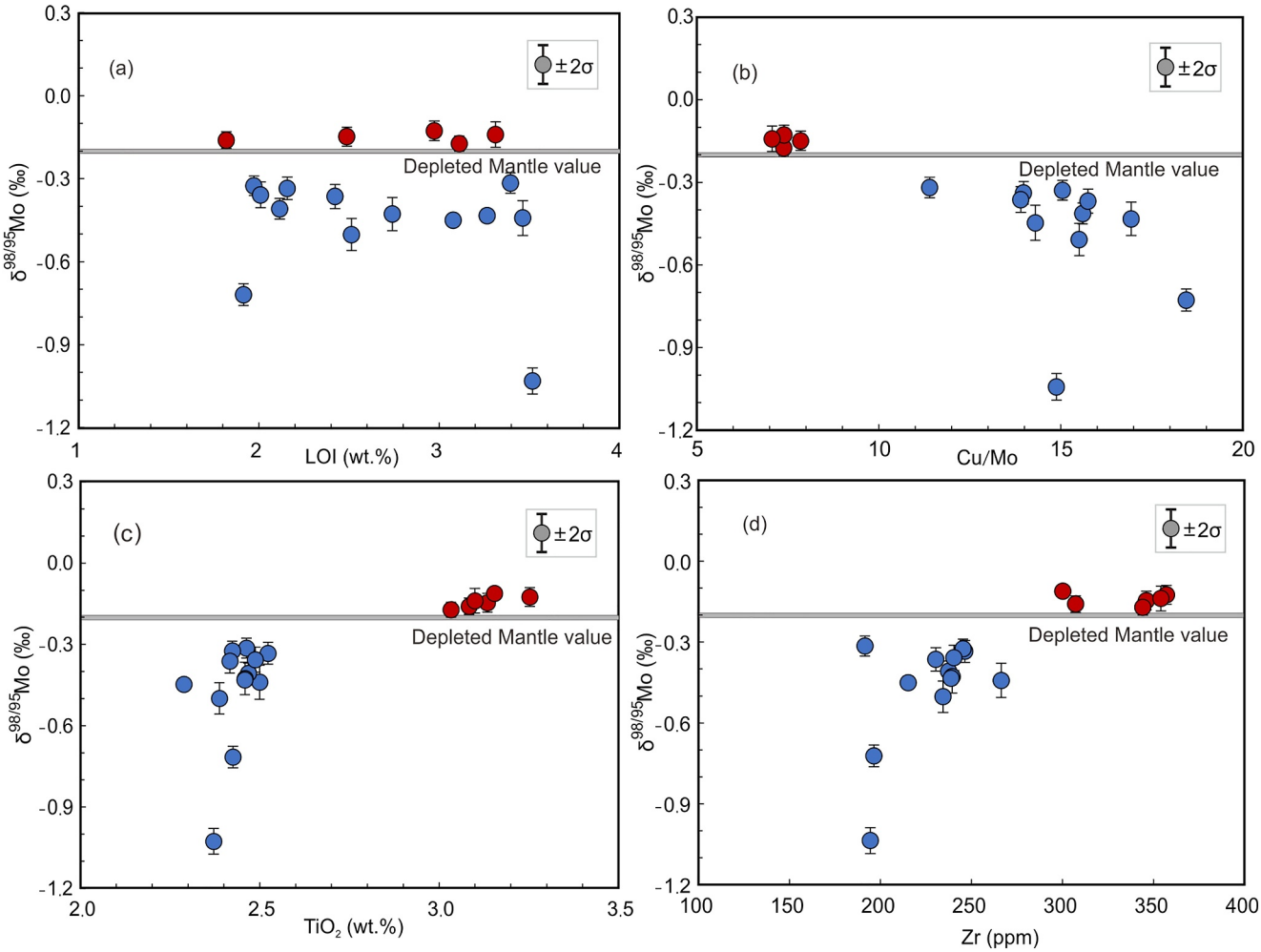

Figure 7. Diagrams of $\delta^{98/95}$Mo (‰) versus (a) LOI; (b) Cu/Mo; (c) TiO_2 (wt.%); (d) Zr (ppm) for Maguan alkali basalts. The $\delta^{98/95}$Mo value of DM is from McCoy-West et al. (2019). Error bars represent the average of two standard deviations (2σ) for $\delta^{98/95}$Mo values, representing long-term precision and accuracy.

(Figure 6). Additionally, the presence of mantle xenoliths in the Maguan basalts further suggests that the process or influence of fractional crystallization is minimal. Therefore, we conclude that the observed Mo isotope variations reflect primary magma or source characteristics rather than being caused by fractional crystallization. Refractory Mo-bearing phases, such as oxides and sulfides, in the mantle source could lead to potential $\delta^{98/95}$Mo fractionation during partial melting. The positive Nb and Ta anomalies in the samples suggest the absence of residual rutile in the mantle source (Figure 4b). Magmatic sulfides, with significantly heavier $\delta^{98/95}$Mo signature compared to coexisting silicate melts (Voegelin et al., 2012) and stronger Cu partitioning relative to Mo (Y. Li & Audétat, 2012), imply that residual sulfides in the mantle source would likely produce lower Cu/Mo and lower $\delta^{98/95}$Mo. Nevertheless, this trend is not evident in our samples (Figure 7b). Thus, residual minerals in the mantle are not the primary factor influencing Mo isotope variations during partial melting.

Low degree melting can induce Mo isotopic fractionation, since Mo^{6+} is more incompatible than Mo^{4+}, resulting in melts with elevated $Mo^{6+}/\Sigma Mo$ ratios compared to the residue, and consequently, heavier $\delta^{98/95}$Mo values (McCoy-West et al., 2019). Given that La and Sm are more incompatible than the heavy rare earth element (REE) Yb during partial mantle melting, the ratios of La/Yb and Sm/Yb are indicative of the degree of partial melting. Based on the trace elemental modeling of a hypothetical peridotite + garnet pyroxenite mantle, type I basalts could be produced at 5%–8% degrees of melting with 10%–30% garnet pyroxenite, while type II basalts are generated by 3%–4% degrees of melting with little to no contribution from garnet pyroxenite (Figure 3d). According to the non-modal batch melting model developed by McCoy-West et al. (2019), our calculated results suggest that Mo isotopic fractionation during partial melting is minimal, with $\Delta^{98/95}$Mo < 0.04‰ for melts

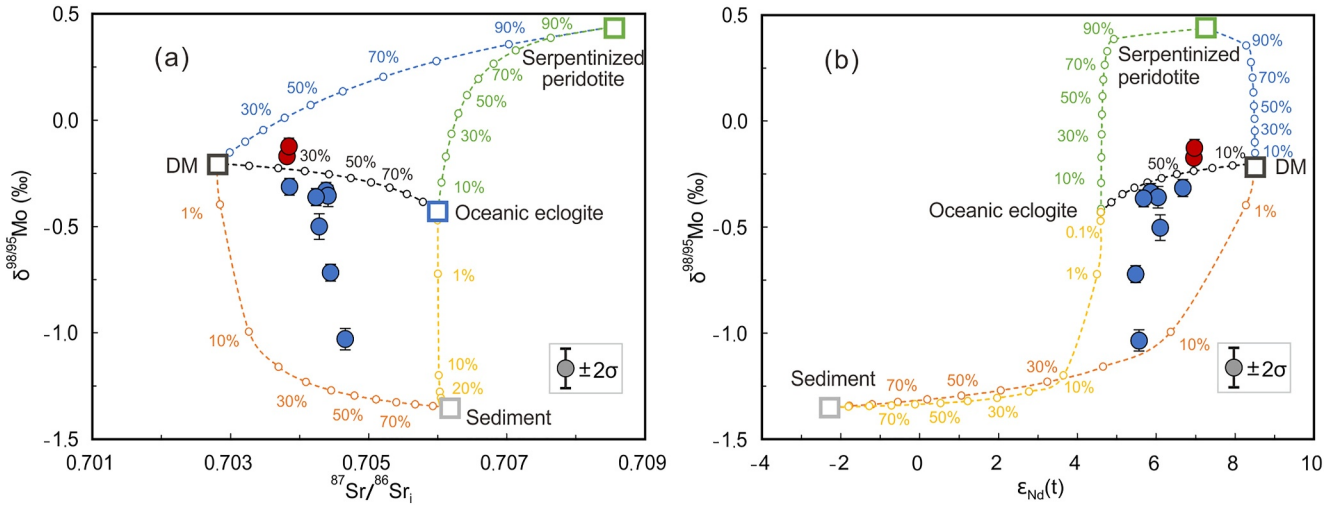

Figure 8. Diagrams of (a) $\delta^{98/95}$Mo versus $^{87}Sr/^{86}Sr_i$, (b) $\delta^{98/95}$Mo versus $\varepsilon_{Nd}(t)$ for Maguan alkali basalts. Data of DM, Oceanic crust and sediment are displayed in Table S5 in Supporting Information S1. Mo isotopic composition of the DM endmember was chosen from Bezard et al. (2016) and McCoy-West et al. (2019). Other isotopic compositions and trace elements of DM are from Gale et al. (2013). Mo content and $\delta^{98/95}$Mo value of oceanic crust are an average value estimated from studies by Chen et al. (2019). The Ce/Mo values, $^{86}Sr/^{87}Sr_i$ and $\varepsilon_{Nd}(t)$ of oceanic crust were chosen within the range of values reported by Yu et al. (2022), Fang, Dai, and Zhao (2023) and reference therein. Other data of oceanic crust were chosen from Frey et al. (1991). Mo content and $\delta^{98/95}$Mo value of sediments endmember were chosen within the range of within range of clay sediments (Freymuth et al., 2015; Gaschnig et al., 2017). Other data of sediments endmembers are from Plank (2014). Mo content and $\delta^{98/95}$Mo value of serpentinized peridotites endmember are average values estimated from studies by Chen et al. (2019) and Rojas-Kolomiets et al. (2023). Other data of serpentinized peridotites endmember are from Frisby et al. (2016a, 2016b). Due to the limited Mo isotope fractionation between mantle source and melts compared to the significant difference between distinct endmembers, we simply present mixing calculations using bulk rocks rather than melts. Input of oceanic eclogite, sediment and serpentinized peridotite into the DM are shown by black, orange and blue dashed lines, respectively, with the tick marks and numbers showing the proportion. Input of sediment and serpentinized peridotite into oceanic eclogite are shown for comparison by yellow and green dashed lines, respectively, with the tick marks and numbers showing the proportion.

fractions of 5%–10% and a $Mo^{6+}/\Sigma Mo$ ratio between 0.90 and 0.99. This result does not explain the isotopically lighter Mo in type I basalts, the significant isotope variations (mean 0.33‰) between the two types of basalts, or the $\delta^{98/95}$Mo variations among type I basalts of comparable melting degrees (Table 1).

Therefore, we propose that mantle melting alone does not account for the Mo isotope compositions of the Maguan alkali basalts, which more plausibly indicate a heterogeneous mantle source. Previous studies have proposed that the Maguan alkali basalts were derived by partial melting of the metasomatized asthenospheric mantle (Lei et al., 2021; S.-A. Liu et al., 2020). The Mo isotopic heterogeneity is more likely ascribed to the variable addition of recycled subducted components.

4.2. Origin of Isotopically Light Mo Component for Type I Basalts

Type I basalts exhibit lower $\delta^{98/95}$Mo values compared to depleted MORB (-0.206 ± 0.02‰, Bezard et al., 2016) and global peridotite xenoliths (-0.206 ± 0.05‰, Liang et al., 2017), indicating that some recycled components with low $\delta^{98/95}$Mo value have contributed to the mantle source. In addition to the necessary depleted asthenospheric mantle (e.g., J. Wang et al., 2024), potential low $\delta^{98/95}$Mo contributors to the continental alkali OIB-like basalts include subcontinental lithospheric mantle (e.g., Z. Wang et al., 2018), recycled basaltic oceanic crust (e.g., Jin et al., 2020; Ma et al., 2022), recycled sediments (e.g., Jin et al., 2020) or subducted oceanic lithosphere.

The subcontinental lithospheric mantle beneath the research area during the Cenozoic era has been well-documented by Eocene-Oligocene potassic magmas in Western Yunnan, volcanic rocks in Tengchong (Guo et al., 2005; X.-L. Huang et al., 2010), and peridotite xenoliths in the Maguan basalts (X.-K. Huang, 2012; C.-Z. Liu et al., 2013). Maguan basalts markedly differ from the magmas in Western Yunnan and Tengchong, which are characterized by negative anomalies in HFSEs such as Nb and Ta and enriched Sr-Nd isotopic signatures (Guo et al., 2005; X.-L. Huang et al., 2010). The Sr-Nd isotopic compositions of peridotite xenoliths in Maguan basalts, like those of MORB (X.-K. Huang, 2012), suggest a depleted refractory lithospheric mantle origin (C.-Z. Liu et al., 2013), and do not account for the characteristics of Maguan alkali basalts. Additionally, the depleted upper mantle has low Mo concentrations (<0.03 ppm, Z. Wang & Becker, 2018). For instance, DM xenoliths from

Kilbourne Hole exhibit extremely low Mo contents (0.04–0.05 ppm, Liang et al., 2017). Given that the highly depleted peridotite xenoliths from Maguan, representing the lithospheric mantle, share similar characteristics with xenoliths from Kilbourne Hole (C.-Z. Liu et al., 2013), we infer that their Mo contents are also low. Other studies of subcontinental lithospheric mantle further support this. For example, the Mo content of the subcontinental lithospheric mantle that produced the Sailipu ultrapotassic rocks is less than 0.022 ppm, as calculated based on data from F. Huang et al. (2023) and C. Sun et al. (2007). Therefore, the low Mo concentrations of the subcontinental lithospheric mantle make it unlikely to significantly influence the Mo content and Mo isotopic composition of the Maguan basalts. Consequently, the subcontinental lithospheric mantle does not contribute to the low-$\delta^{98/95}$Mo end member in the source of Maguan basalts.

During subduction, hydrous minerals in the oceanic crust break down and release fluids (Peacock, 1990). Mo is fluid-mobile and heavier Mo isotopes are inclined to partition into fluids because ^{98}Mo prefers tetrahedral coordination in fluids, while ^{95}Mo preferentially retains octahedral sites in minerals such as rutile and sulfides. This is corroborated by arc lava (Freymuth et al., 2015; König et al., 2016; Voegelin et al., 2014; Wille et al., 2018), which are Mo-enriched and have $\delta^{98/95}$Mo values higher than depleted MORB (Bezard et al., 2016) and most oceanic sediments (Freymuth et al., 2015). Consequently, the residual slab, particularly residual eclogites, are left with a comparatively isotopically lighter Mo and high Ce/Mo ratios. This is evidenced by the isotopically light Mo composition found in rutile (Chen et al., 2019), a frequent accessory phase in the mafic subducted crust. Additionally, eclogites, being dehydrated and partially melted residues of subducted oceanic crust, typically exhibit very light Mo isotopic compositions. This is well-documented by Chen et al. (2019) and Ahmad et al. (2021), who analyzed exhumed MORB-type eclogites and found $\delta^{98/95}$Mo values as low as $-0.68‰$ and $-1.01‰$, respectively. Furthermore, the Ce/Mo ratios in these eclogites are notably high (up to 250, Chen et al., 2019). Consequently, the partial melting of recycled eclogites in the mantle source could potentially produce melts with low $\delta^{98/95}$Mo values and high Ce/Mo ratios, mirroring the key geochemical characteristics observed in our samples. The $\delta^{98/95}$Mo and Ce/Mo values in Maguan basalts closely resemble those of MORB-type eclogites (Figure 6). The super-chondritic Nb/Ta (15.7–21) and Nb/La (1.97–3.17) ratios observed in the Maguan basalts suggest that their mantle source likely includes contributions from partial melts of rutile-bearing eclogites (Foley et al., 2002; Rudnick et al., 2000). Therefore, MORB-type eclogites have played a significant role in the mantle source of type I basalts. If the light Mo isotope composition were solely due to contributions from oceanic crust, we would expect a negative correlation between Mo isotope values and TiO_2 or Zr content due to the involvement of rutile. However, no such correlation is observed in our samples (Figures 7c and 7d), indicating that rutile-bearing eclogites are not the sole source of the isotopically light Mo composition. Moreover, the relatively enriched Sr-Nd isotopic compositions of type I basalts cannot be easily explained by a contribution from dehydrated oceanic crust.

Other subducted materials with much lower $\delta^{98/95}$Mo values may have also contributed. Mo is a multi-valent element and sensitive to redox (Anbar, 2004; Leitzke et al., 2017). Thus, sediments deposited in different redox environments show variable Mo isotope compositions due to mass-dependent isotopic fractionation during low-temperature processes. Marine sediment samples from various ocean drilling sites display a range of $\delta^{98/95}$Mo values, with certain pelagic sediments showing extremely low $\delta^{98/95}$Mo values, reaching $-1.87‰$ (Freymuth et al., 2015). The interaction with sediment-derived melts is postulated to contribute to isotopically light Mo in certain arc lava (Freymuth et al., 2015; König et al., 2016). Casalini et al. (2019) and F. Huang et al. (2023) also attribute the low $\delta^{98/95}$Mo values in mafic ultra-potassic volcanic rocks to sediment melt contributions. Therefore, marine sediments are suitable candidates for the source of isotopically light Mo. The negative correlation between $\delta^{98/95}$Mo values and $^{87}Sr/^{86}Sr_i$ ratios and positive correlations between $\delta^{98/95}$Mo values and $\varepsilon_{Nd}(t)$ values (Figure 8) also corroborate the idea that sediments contributed to the isotopically lighter Mo source.

However, negative Nb and Ta anomalies in sediment melts (Plank, 2014) cannot account for the positive Nb and Ta anomalies observed in the Maguan basalts. Thus, contributions from both eclogites and sediments to the isotopically light Mo composition are essential. We present mixing calculations between DM, subducted oceanic eclogites, and subducted sediments to explain the Mo isotopes and Sr-Nd isotopes for the Maguan basalts (Figure 8). The mixing lines of the three end members fully encompass the Mo and Sr-Nd isotopic characteristics of Maguan type I basalts. The mixing model shows that melts from subducted sediments and eclogites, which are less basic than melts of mantle peridotites, have influenced the mantle source of the type I basalts, resulting in a mantle source of hybrid pyroxenites and peridotites. This inference is also consistent with the major and trace

element characteristics of the whole rocks and olivine from the basalts (Figures 3b–3d; Bowman & Ducea, 2023). In summary, the Mo isotopes of our samples reflect the mantle lithological heterogeneity that the pyroxenites contribute to the source for Maguan type I basalts.

4.3. Origin of Isotopically Heavy Mo Component for Type II Basalts

Maguan type II basalts exhibit $\delta^{98/95}$Mo values reaching as high as −0.11‰. While the $\delta^{98/95}$Mo values of type II basalts align with those of DM, the OIB-like REEs and trace element patterns (Figure 4) indicate that DM alone cannot be the sole mantle source. The presence of isotopically heavy Mo in these basalts cannot be solely attributed to the addition of dehydrated oceanic crust to the mantle, as it is known to possess isotopically light Mo as mentioned above (Chen et al., 2019; Freymuth et al., 2015). Considering the effect of slab dehydration, which could decrease $\delta^{98/95}$Mo by ∼0.4‰ or more in subducted materials (Chen et al., 2019), an end-member with isotopically heavier Mo is necessary to account for the Mo isotopic signatures of type II basalts.

Subducted sediments globally are complex and display a variety of Mo isotopic compositions, including some with low $\delta^{98/95}$Mo values, but many sediments show isotopically heavy Mo. Mo is incorporated from seawater into sediments in anoxic environments with minimal isotopic fractionation (Barling et al., 2001; Neubert et al., 2008), leading to isotopically heavy Mo in black shales ($\delta^{98/95}$Mo values range mostly from 0‰ to +1.7‰, Freymuth et al., 2016). Marine carbonates are also distinguished by high $\delta^{98/95}$Mo values (+1.66 ± 1.05‰) and low Ce/Mo ratios (average 1.4), as reported by Y. Zhang et al. (2020) and references therein. Continental margin sediments also possess isotopically heavy Mo, a characteristic attributable to reducing depositional environments and high primary oceanic productivity (Kendall et al., 2017). Consequently, these sediments appear to be viable candidates as a source of isotopically heavy Mo. However, the elevated $\delta^{98/95}$Mo values in Maguan type II basalts are coupled with low $^{87}Sr/^{86}Sr$ ratios and high $\varepsilon_{Nd}(t)$ values, which argue against a contribution from subducted sediments to the isotopically heavier Mo source.

Serpentinized peridotites, which exhibit high $\delta^{98/95}$Mo values (0.13‰, Chen et al., 2019) and low Ce/Mo ratios (<2.5, Chen et al., 2019), may serve as potential candidates for an end-member with isotopically heavier Mo. Serpentinite likely constitutes a part of the subducting slab, functioning either as the descending oceanic lithosphere at the slab's base or as the fore-arc mantle wedge drawn downward at the slab's uppermost portion (Spandler & Pirard, 2013). Interaction with isotopically heavy seawater ($\delta^{98/95}$Mo = ∼2.3‰, Barling et al., 2001) during serpentinization results in high $\delta^{98/95}$Mo values in serpentinites (>0.1‰, Chen et al., 2019). Although oceanic crust may be dehydrated efficiently during subduction, thus losing fluid-mobile elements and isotopically heavy Mo, serpentinites associated with oceanic crust may carry fluid-mobile elements and isotopically heavy Mo into the deep mantle (Deschamps et al., 2013). An underlying serpentinized slab mantle is an appealing source for Maguan type II basalts because the top of the subducting slab would fully dehydrate before reaching sub-arc depth (Syracuse et al., 2010; van Keken et al., 2011; Wada et al., 2012). Moreover, the oldest core of the slab comprising a serpentinized lithospheric mantle could be transported into the deep mantle before complete dehydration due to the stabilization of antigorite serpentine at depths shallower than 250 km, according to an experimental study reported by Hilairet et al. (2006). Serpentinized mantle peridotites have $\delta^{98/95}$Mo values between −0.09 and 1.10‰ and Ce/Mo ratios from 0.01 to 2.06 (Chen et al., 2019; Rojas-Kolomiets et al., 2023). This characteristic establishes a noticeable correlation with enhanced $\delta^{98/95}$Mo values as well as lowered Ce/Mo, and increased Ba/Th ratios, which are prominent in our type II samples (Figures 5a and 6; Table 1). Serpentinized peridotites are enriched in fluid-mobile elements such as Ba, Sr, and LREE due to the introduction of fluids during the serpentinization process. The overall higher concentrations of trace elements and REEs in type II basalts, compared to type I basalts, indicate a greater contribution of serpentinized peridotite in their source (Figure 4). In particular, the significantly higher Ba and Sr contents in Maguan type II basalts further support this scenario (Table S2 in Supporting Information S1).

We present mixing calculations between DM, subducted oceanic eclogites, and serpentinized peridotites to explain the Mo isotopes and Sr-Nd isotopes for Maguan basalts. These calculations can fully explain the Mo, Sr and Nd isotopic compositions of Maguan type II basalts (Figure 8). The Mo isotopic characteristics confirm the contribution of serpentinized peridotites to their source region. The contribution of serpentinized peridotites may be small, but it is crucial to balance the isotopically light Mo of the oceanic crust and drives the Mo isotopic values of Maguan type II basalts to approach or even slightly exceed those of DM. Their Sr and Nd isotope ratios are similar to those of MORB, indicating a significant contribution from depleted peridotite mantle and less

contribution from sediments and oceanic crust melts compared to type I basalts. Their major and trace elements also point to a predominantly peridotite mantle source (Figures 3b–3d; Bowman & Ducea, 2023). In this regard, the Mo isotope compositions of our samples reflect mantle lithological heterogeneity where pyroxenites may contribute less to the source for Maguan type II basalts compared to the source for type I basalts.

4.4. Tectonic Implications for Southeastern Margin of Tibetan Plateau

As shown above, the mantle source of type I basalts involved recycled eclogites and sediment melts, whereas the mantle source of type II basalts mainly contained recycled serpentinized peridotites. The melting of residual oceanic crust and sediments together resulted in less basic melts which then reacted with the asthenospheric mantle to generate mafic-ultramafic metasomatites containing pyroxenites and correspond to the source of type I basalts. Residual serpentinized peridotites-derived melts, together with oceanic crust-derived melts, reacted with the overlying mantle, generating the mantle source of Maguan type II basalts. Seismic tomographic images show the presence of a high-velocity slab at depths of 410–660 km beneath the Maguan area (Figure 1c; J. Huang & Zhao, 2006), which is most likely to be the source of the oceanic crust, sediments and serpentinized oceanic lithosphere metasomatizing the DM in Maguan. Our research findings suggest that the stagnant slab could not have originated from the Indian continental plate. Based on the low $^{207}Pb/^{206}Pb$ (15.5–15.7) and the relatively invariant Sr and Nd isotopes of the Maguan basalts, it is suggested that the source is less than 500 million years old. Considering the complex geological records of Neo-Tethys (since the Cretaceous), Paleo-Tethys (Devonian-Triassic) and Proto-Tethys (Late Sinian-Silurian) oceans at the southeastern margin of the Tibetan Plateau (e.g., Deng et al., 2014, 2018; Nie et al., 2015), the origin of the residual slab in the deep mantle may be linked to the subduction of one or more of the aforementioned oceanic plates.

Cenozoic activities on the southeastern margin of the Tibetan Plateau occurred in two episodes with distinct geochemical signatures at 42-24 Myr and 16-0 Myr. Combined trace-elemental and isotopic characteristics indicate that the 42-24 Myr high-potassic magmas are derived from a metasomatized subcontinental lithospheric mantle source (e.g., J. Wang et al., 2022; J.-H. Wang et al., 2001), while the younger type of magmas, including the Maguan basalts, are from the asthenospheric mantle. Therefore, the enriched mantle that existed beneath the southeastern margin of the Tibetan Plateau during the Eocene–Oligocene has been replaced by upwelling depleted and juvenile asthenospheric mantle during the Cenozoic, consistent with a Re-Os isotopic study of mantle xenoliths in Maguan basalts by C.-Z. Liu et al. (2013). The replacement of the lithospheric mantle in the Maguan region indicates that a geodynamic mechanism similar to the one responsible for the destruction of the North China Craton is also active in southwestern China.

The subduction of the Western Pacific plate is considered to be the main dynamic factor in the destruction of the North China Craton (Zhu et al., 2012). Considering the similar major and trace element and isotopic compositions of Cenozoic alkali basalts in Eastern China and Maguan basalts (Figures 3a, 5a, 5c, and 6), the main dynamic factor that promoted formation of the Maguan basalts may be related to the subduction of a particular plate. Moreover, it is suggested that arc magmas could have formed at the North Australian continental lithosphere edge when it plowed through the mantle above the detached Arafura slab remnant (van Hinsbergen et al., 2020). Considering the Maguan alkali basalts along with other widespread Miocene magmatic rocks and tectonic events, such as faults and rifts across the Tibetan Plateau and its surroundings (e.g., Blisniuk et al., 2001; Hao et al., 2022; Yin & Taylor, 2011), Miocene magmatic and tectonic activity in the region seem to have been governed by a large-scale geodynamic event related to plate subduction (van Hinsbergen, 2022). Seismological images reveal that the Himalayan slab is currently steeply subducted below Tibet and has reached the MTZ (Hou et al., 2024; van Hinsbergen, 2022). Therefore, Maguan Miocene volcanic rocks may derived from a previously subduction-enriched asthenospheric source that was stirred by the underthrusting of the Burma plate, a part of the Himalayan slab, which is also consistent with the geophysical observations (Figure 1c).

4.5. Implications for Mo Isotopic Heterogeneity of OIB-Like Alkali Basalts

Compared to arc basalts ($\delta^{98/95}Mo = -0.10 \pm 0.02‰$, Fang, Dai, & Zhao, 2023 and references therein), OIBs ($\delta^{98/95}Mo = -0.59‰$ to $+0.10‰$, Fang, Dai, & Zhao, 2023 and references therein) show large variations in terms of Mo isotopic composition. The Mo isotopic compositions of OIB-like continental basalts also show large variations with $\delta^{98/95}Mo$ ranging from $-0.53‰$ to $0.09‰$ (Fang, Dai, Zheng, & Zhao, 2023) in basalts from Eastern China and $-0.4‰$ to $-0.08‰$ (Y. Zhang et al., 2019) in basalts from Western China. Although most of

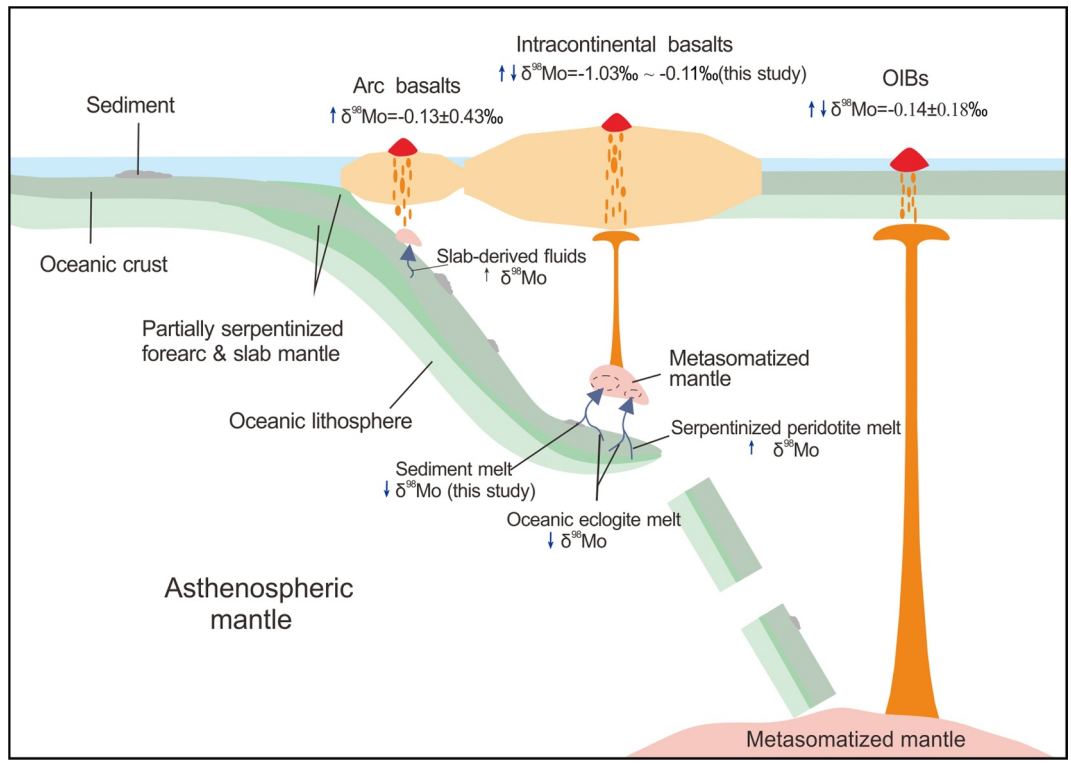

Figure 9. A cartoon system model showing the recycling of complex material composition of oceanic slabs as tracked by Mo isotope evidence from intra-continental mantle-derived magmas. The Mo isotopes of arc basalts and oceanic island basalts are from Fang, Dai, and Zhao (2023) and references therein.

the OIB-like continental basalts have $\delta^{98/95}$Mo values lower than those of the DM, a significant proportion have similar or even higher $\delta^{98/95}$Mo values than the mantle, which is consistent with our samples ($\delta^{98/95}$Mo = −1.03‰ to −0.11‰).

Isotopically light Mo in OIBs and OIB-like continental basalts is commonly believed to be predominantly influenced by contribution from dehydrated subducting oceanic crust (Ma et al., 2022; Willbold & Elliott, 2023). However, dehydrated oceanic crust in the form of eclogites fails to explain the extreme isotopically light Mo, because the lowest $\delta^{98/95}$Mo value of oceanic eclogites reported so far is −1.01‰ (Ahmad et al., 2021), higher than the lowest $\delta^{98/95}$Mo values (−1.03‰) of Maguan basalts. Some sediments with extremely isotopically light Mo must also have contributed to such basalts. Accordingly, a variety of pyroxenite signals, generated by reactions between sediments, oceanic crust melts and ambient mantle, exist in mantle sources of OIB-like continental basalts. Given the wide variations in Mo isotopes in sediments, certain subducted sediments, such as black shales (Freymuth et al., 2016) and carbonates (Y. Zhang et al., 2020), can also contribute to the isotopically heavy Mo composition of intracontinental OIB-like basalts. Some studies have already attributed the isotopically heavy Mo to sediments (Fu et al., 2023; Y. Zhang et al., 2020). However, the negative correlation between $\delta^{98/95}$Mo values and $^{87}Sr/^{86}Sr$ and positive correlation between $\delta^{98/95}$Mo values and $\varepsilon_{Nd}(t)$, however, exclude the contribution of sediments to the isotopically heavy Mo of the Maguan basalts. Serpentinized peridotites can also contribute to the isotopically heavy Mo composition of intraplate OIBs (Fang, Dai, & Zhao, 2023). This appears to be the case for Maguan type II basalts because they show higher $\delta^{98/95}$Mo values than DM, lower Ce/Mo ratios and are more depleted than the type I basalts, consistent with dominant peridotites in their mantle source.

Our study on Maguan intra-continental alkali basalts supports a model where recycled oceanic crust and sediments are responsible for isotopically light Mo compositions in the source of intra-continental basalts (Figure 9). Meanwhile, the extremely isotopically heavy Mo in some intra-continental basalts is mainly attributable to serpentinized peridotites (Figure 9). In summary, the heterogeneity in Mo isotopes in intraplate basalts arises from the heterogeneity of subducted materials, primarily due to the compositional differences between oceanic crust, sediments and serpentinized oceanic lithospheric mantle. Mo isotopic system serves as an efficient way to trace

subducted materials and decode mantle heterogeneity, which traditional radiogenic isotopic methods like Sr-Nd-Pb might not resolve. At any point in time, the mantle is extremely heterogeneous in terms of Mo isotopes, even over limited areas, which may provide an effective way to resolve complex geodynamic events of the past.

5. Conclusions

1. Miocene (~13–11 Ma) Maguan intraplate alkali basalts are characterized by OIB-like trace-element patterns and depleted Sr-Nd-Pb isotope compositions. These samples are divided into two groups based on petrographic observation and geochemical features.
2. Type I basalts, characterized by low $\delta^{98/95}$Mo values, may originate from a DM metasomatized by melts from recycled dehydrated oceanic crust and sediments. The type II basalts with higher $\delta^{98/95}$Mo values may be derived from a DM metasomatized by melts from subducted serpentinized peridotites.
3. The stagnant Tethys oceanic slabs in the deep mantle of the Maguan area have supplied significant materials to the mantle source of the Maguan alkali basalts.
4. West Burma plate subduction-induced mantle upwelling is a likely mechanism for the generation of Maguan alkali basalts.
5. The mantle heterogeneity in Mo isotopic composition makes Mo isotopes effective tools in deciphering recycled components.

Data Availability Statement

Data used in this work are available at D. Xu et al. (2024).

Acknowledgments
We are very grateful to the editor Professor Paul D. Asimow, associate editor Professor Lingsen Zeng and two anonymous reviewers for their detailed and constructive comments, which greatly improved the manuscript. We appreciate the assistance of Wanfeng Zhang, Xinyu Wang and Wenhua Cao for Ar-Ar dating and whole-rock and olivine major element analyses, respectively. The financial support for this research was provided by the National Natural Science Foundation of China (No. 42021002) and the Second Tibetan Plateau Scientific Expedition and Research (STEP) (2019QZKK0702). This is contribution No. IS-3568 from GIGCAS.

References

Ahmad, Q., Wille, M., König, S., Rosca, C., Hensel, A., Pettke, T., & Hermann, J. (2021). The Molybdenum isotope subduction recycling conundrum: A case study from the Tongan subduction zone, Western Alps and Alpine Corsica. *Chemical Geology*, *576*, 120231. https://doi.org/10.1016/j.chemgeo.2021.120231

Anbar, A. D. (2004). Molybdenum stable isotopes: Observations, interpretations and directions. *Reviews in Mineralogy and Geochemistry*, *55*(1), 429–454. https://doi.org/10.2138/gsrmg.55.1.429

Barling, J., Arnold, G. L., & Anbar, A. D. (2001). Natural mass-dependent variations in the isotopic composition of molybdenum. *Earth and Planetary Science Letters*, *193*(3–4), 447–457. https://doi.org/10.1016/S0012-821X(01)00514-3

Bezard, R., Fischer-Gödde, M., Hamelin, C., Brennecka, G. A., & Kleine, T. (2016). The effects of magmatic processes and crustal recycling on the molybdenum stable isotopic composition of Mid-Ocean Ridge Basalts. *Earth and Planetary Science Letters*, *453*, 171–181. https://doi.org/10.1016/j.epsl.2016.07.056

Blisniuk, P. M., Hacker, B. R., Glodny, J., Ratschbacher, L., Bi, S., Wu, Z., et al. (2001). Normal faulting in central Tibet since at least 13.5 Myr ago. *Nature*, *412*(6847), 628–632. https://doi.org/10.1038/35088045

Bowman, E. E., & Ducea, M. N. (2023). Pyroxenites melting at subduction zones. *Geology*, *51*(4), 383–386. https://doi.org/10.1130/G50929.1

Casalini, M., Avanzinelli, R., Tommasini, S., Elliott, T., & Conticelli, S. (2019). Ce/Mo and molybdenum isotope systematics in subduction-related orogenic potassic magmas of Central-Southern Italy. *Geochemistry, Geophysics, Geosystems*, *20*(6), 2753–2768. https://doi.org/10.1029/2019GC008193

Chen, S., Hin, R. C., John, T., Brooker, R., Bryan, B., Niu, Y., & Elliott, T. (2019). Molybdenum systematics of subducted crust record reactive fluid flow from underlying slab serpentine dehydration. *Nature Communications*, *10*(1), 4773. https://doi.org/10.1038/s41467-019-12696-3

Chen, S., Sun, P., Niu, Y., Guo, P., Elliott, T., & Hin, R. C. (2022). Molybdenum isotope systematics of lavas from the East Pacific Rise: Constraints on the source of enriched mid-ocean ridge basalt. *Earth and Planetary Science Letters*, *578*, 117283. https://doi.org/10.1016/j.epsl.2021.117283

Cheng, Z., Zhang, Z., Wang, Z., Jin, Z., Hao, J., Jin, L., & Santosh, M. (2022). Petrogenesis of continental intraplate alkaline basalts in the Tuoyun Basin, western Central Asian Orogenic Belt: Implications for deep carbon recycling. *Journal of Petrology*, *63*(9), egac088. https://doi.org/10.1093/petrology/egac088

Chung, S.-L., Lee, T.-Y., Lo, C.-H., Wang, P.-L., Chen, C.-Y., Yem, N. T., et al. (1997). Intraplate extension prior to continental extrusion along the Ailao Shan-Red River shear zone. *Geology*, *25*(4), 311–314. https://doi.org/10.1130/0091-7613(1997)025<0311:IEPTCE>2.3.CO;2

Deng, J., Wang, C., Zi, J.-W., Xia, R., & Li, Q. (2018). Constraining subduction-collision processes of the Paleo-Tethys along the Changning–Menglian Suture: New zircon U-Pb ages and Sr–Nd–Pb–Hf–O isotopes of the Lincang Batholith. *Gondwana Research*, *62*, 75–92. https://doi.org/10.1016/j.gr.2017.10.008

Deng, J., Wang, Q., Li, G., & Santosh, M. (2014). Cenozoic tectono-magmatic and metallogenic processes in the Sanjiang region, southwestern China. *Earth-Science Reviews*, *138*, 268–299. https://doi.org/10.1016/j.earscirev.2014.05.015

Deschamps, F., Godard, M., Guillot, S., & Hattori, K. (2013). Geochemistry of subduction zone serpentinites: A review. *Lithos*, *178*, 96–127. https://doi.org/10.1016/j.lithos.2013.05.019

Doucet, L. S., Li, Z.-X., Gamal El Dien, H., Pourteau, A., Murphy, J. B., Collins, W. J., et al. (2020). Distinct formation history for deep-mantle domains reflected in geochemical differences. *Nature Geoscience*, *13*(7), 511–515. https://doi.org/10.1038/s41561-020-0599-9

Elliott, T., Thomas, A., Jeffcoate, A., & Niu, Y. (2006). Lithium isotope evidence for subduction-enriched mantle in the source of mid-ocean-ridge basalts. *Nature*, *443*(7111), 565–568. https://doi.org/10.1038/nature05144

Eriksen, Z. T., & Jacobsen, S. B. (2022). Calcium isotope constraints on OIB and MORB petrogenesis: The importance of melts mixing. *Earth and Planetary Science Letters*, *593*, 117665. https://doi.org/10.1016/j.epsl.2022.117665

Fang, W., Dai, L.-Q., & Zhao, Z.-F. (2023). Molybdenum isotopic heterogeneity for intraplate basalts and its origin. *Chemical Geology*, *641*, 121784. https://doi.org/10.1016/j.chemgeo.2023.121784

Fang, W., Dai, L.-Q., Zheng, Y.-F., & Zhao, Z.-F. (2023). Molybdenum isotopes in mafic igneous rocks record slab-mantle interactions from subarc to postarc depths. *Geology*, *51*(1), 3–7. https://doi.org/10.1130/G50456.1

Flower, M. F. J., Hoàng, N., Lo, C.-H., Chí, C. T., Cu'ò'ng, N. Q., Liu, F.-T., et al. (2013). Potassic magma genesis and the Ailao Shan-Red River fault. *Journal of Geodynamics*, *69*, 84–105. https://doi.org/10.1016/j.jog.2012.06.008

Foley, S., Tiepolo, M., & Vannucci, R. (2002). Growth of early continental crust controlled by melting of amphibolite in subduction zones. *Nature*, *417*(6891), 837–840. https://doi.org/10.1038/nature00799

Frey, F. A., Jones, W. B., Davies, H. L., & Weis, D. A. M. (1991). Geochemical and petrologic data for basalts from Sites 756, 757, and 758: Implications for the origin and evolution of the Ninetyeast Ridge. *Proceedings of the Ocean Drilling Program, Scientific Results*, *121*, 611–659. https://doi.org/10.2973/odp.proc.sr.121.163.1991

Freymuth, H., Elliott, T., van Soest, M., & Skora, S. (2016). Tracing subducted black shales in the Lesser Antilles arc using molybdenum isotope ratios. *Geology*, *44*(12), 987–990. https://doi.org/10.1130/G38344.1

Freymuth, H., Vils, F., Willbold, M., Taylor, R. N., & Elliott, T. (2015). Molybdenum mobility and isotopic fractionation during subduction at the Mariana arc. *Earth and Planetary Science Letters*, *432*, 176–186. https://doi.org/10.1016/j.epsl.2015.10.006

Frisby, C., Bizimis, M., & Mallick, S. (2016a). Hf–Nd isotope decoupling in bulk abyssal peridotites due to serpentinization. *Chemical Geology*, *440*, 60–72. https://doi.org/10.1016/j.chemgeo.2016.07.006

Frisby, C., Bizimis, M., & Mallick, S. (2016b). Seawater-derived rare earth element addition to abyssal peridotites during serpentinization. *Lithos*, *248–251*, 432–454. https://doi.org/10.1016/j.lithos.2016.01.025

Fu, X., Fang, W., Dai, L.-Q., Zhao, Z.-F., Gong, B., & Zheng, Y.-F. (2023). Mo isotopes record recycling of anoxic sediments in a Paleo-oceanic subduction zone. *Chemical Geology*, *640*, 121734. https://doi.org/10.1016/j.chemgeo.2023.121734

Gale, A., Dalton, C. A., Langmuir, C. H., Su, Y., & Schilling, J.-G. (2013). The mean composition of ocean ridge basalts. *Geochemistry, Geophysics, Geosystems*, *14*(3), 489–518. https://doi.org/10.1029/2012GC004334

Gamal El Dien, H., Doucet, L. S., Murphy, J. B., & Li, Z.-X. (2020). Geochemical evidence for a widespread mantle re-enrichment 3.2 billion years ago: Implications for global-scale plate tectonics. *Scientific Reports*, *10*(1), 9461. https://doi.org/10.1038/s41598-020-66324-y

Gaschnig, R. M., Reinhard, C. T., Planavsky, N. J., Wang, X., Asael, D., & Chauvel, C. (2017). The molybdenum isotope system as a tracer of slab input in subduction zones: An example from Martinique, Lesser Antilles Arc. *Geochemistry, Geophysics, Geosystems*, *18*(12), 4674–4689. https://doi.org/10.1002/2017GC007085

Gilley, L. D., Harrison, T. M., Leloup, P. H., Ryerson, F. J., Lovera, O. M., & Wang, J.-H. (2003). Direct dating of left-lateral deformation along the Red River shear zone, China and Vietnam. *Journal of Geophysical Research*, *108*(B2), 2127. https://doi.org/10.1029/2001JB001726

Guo, Z., Hertogen, J., Liu, J., Pasteels, P., Boven, A., Punzalan, L. E. A., et al. (2005). Potassic magmatism in western Sichuan and Yunnan provinces, SE Tibet, China: Petrological and geochemical constraints on petrogenesis. *Journal of Petrology*, *46*(1), 33–78. https://doi.org/10.1093/petrology/egh061

Hao, L.-L., Wang, Q., Kerr, A. C., Wei, G.-J., Huang, F., Zhang, M.-Y., et al. (2022). Contribution of continental subduction to very light B isotope signatures in post-collisional magmas: Evidence from southern Tibetan ultrapotassic rocks. *Earth and Planetary Science Letters*, *584*, 117508. https://doi.org/10.1016/j.epsl.2022.117508

Hilairet, N., Daniel, I., & Reynard, B. (2006). Equation of state of antigorite, stability field of serpentines, and seismicity in subduction zones. *Geophysical Research Letters*, *33*(2), L02302. https://doi.org/10.1029/2005GL024728

Hin, R. C., Hibbert, K. E. J., Chen, S., Willbold, M., Andersen, M. B., Kiseeva, E. S., et al. (2022). The influence of crustal recycling on the molybdenum isotope composition of the Earth's mantle. *Earth and Planetary Science Letters*, *595*, 117760. https://doi.org/10.1016/j.epsl.2022.117760

Hofmann, A. W. (1997). Mantle geochemistry: The message from oceanic volcanism. *Nature*, *385*(6613), 219–229. https://doi.org/10.1038/385219a0

Hou, Z., Liu, L., Zhang, H., Xu, B., Wang, Q., Yang, T., et al. (2024). Cenozoic eastward growth of the Tibetan Plateau controlled by tearing of the Indian slab. *Nature Geoscience*, *17*(3), 255–263. https://doi.org/10.1038/s41561-024-01382-9

Huang, F., Li, J., Xu, J., Chen, J., Wang, B., Hu, P., et al. (2023). Mo isotopes archive oceanic sediments in post-orogenic lithospheric mantle. *Geochimica et Cosmochimica Acta*, *341*, 75–89. https://doi.org/10.1016/j.gca.2022.11.023

Huang, J., & Zhao, D. (2006). High-resolution mantle tomography of China and surrounding regions. *Journal of Geophysical Research*, *111*(B9), B09305. https://doi.org/10.1029/2005JB004066

Huang, X.-K. (2012). *The petrological and geochemical characteristics of Cenozoic basalts and mantle-derived xenoliths from Maguan and Pingbian area, Southeastern Yunnan Province and its significance of deep geodynamics*. (in Chinese with English abstract) [Doctoral dissertation]. Retrieved from CNKI database. China University of Geosciences.

Huang, X.-K., Mo, X.-X., Yu, X.-H., Li, Y., & He, W.-Y. (2013). Geochemical characteristics and geodynamic significance of Cenozoic basalts from Maguan and Pingbian, southeastern Yunnan Province. (in Chinese with English abstract). *Acta Petrologica Sinica*, *29*, 1325–1337.

Huang, X.-L., Niu, Y., Xu, Y.-G., Chen, L.-L., & Yang, Q.-J. (2010). Mineralogical and geochemical constraints on the petrogenesis of post-collisional potassic and ultrapotassic rocks from western Yunnan, SW China. *Journal of Petrology*, *51*(8), 1617–1654. https://doi.org/10.1093/petrology/egq032

Jackson, M. G., Hart, S. R., Konter, J. G., Kurz, M. D., Blusztajn, J., & Farley, K. A. (2014). Helium and lead isotopes reveal the geochemical geometry of the Samoan plume. *Nature*, *514*(7522), 355–358. https://doi.org/10.1038/nature13794

Jackson, M. G., Hart, S. R., Koppers, A. A. P., Staudigel, H., Konter, J., Blusztajn, J., et al. (2007). The return of subducted continental crust in Samoan lavas. *Nature*, *448*(7154), 684–687. https://doi.org/10.1038/nature06048

Ji, W.-Q., Wu, F.-Y., Chung, S.-L., Wang, X.-C., Liu, C.-Z., Li, Q.-L., et al. (2016). Eocene Neo-Tethyan slab breakoff constrained by 45 Ma oceanic island basalt–type magmatism in southern Tibet. *Geology*, *44*(4), 283–286. https://doi.org/10.1130/G37612.1

Jin, Q.-Z., Huang, J., Liu, S.-C., & Huang, F. (2020). Magnesium and zinc isotope evidence for recycled sediments and oceanic crusts in the mantle sources of continental basalts from eastern China. *Lithos*, *370–371*, 105627. https://doi.org/10.1016/j.lithos.2020.105627

Kendall, B., Dahl, T. W., & Anbar, A. D. (2017). The stable isotope geochemistry of molybdenum. *Reviews in Mineralogy and Geochemistry*, *82*(1), 683–732. https://doi.org/10.2138/rmg.2017.82.16

König, S., Wille, M., Voegelin, A., & Schoenberg, R. (2016). Molybdenum isotope systematics in subduction zones. *Earth and Planetary Science Letters*, *447*, 95–102. https://doi.org/10.1016/j.epsl.2016.04.033

Le Bas, M. J., Le Maitre, R. W., Streckeisen, A., & Zanettin, B. (1986). A chemical classification of volcanic rocks based on the total alkali-silica diagram. *Journal of Petrology*, *27*(3), 745–750. https://doi.org/10.1093/petrology/27.3.745

Lei, H., Zhao, Z., Niu, Y., Zhang, S., Cousens, B., Ma, Q., et al. (2021). Identifying deep recycled carbonates through Miocene basalts in the Maguan area, SE Tibetan Plateau. *Lithos*, *400–401*, 106356. https://doi.org/10.1016/j.lithos.2021.106356

Leitzke, F. P., Fonseca, R. O. C., Sprung, P., Mallmann, G., Lagos, M., Michely, L. T., & Münker, C. (2017). Redox dependent behavior of molybdenum during magmatic processes in the terrestrial and lunar mantle: Implications for the Mo/W of the bulk silicate Moon. *Earth and Planetary Science Letters*, *474*, 503–515. https://doi.org/10.1016/j.epsl.2017.07.009

Li, C., van der Hilst, R. D., Meltszer, A. S., & Engdahl, E. R. (2008). Subduction of the Indian lithosphere beneath the Tibetan Plateau and Burma. *Earth and Planetary Science Letters*, *274*(1–2), 157–168. https://doi.org/10.1016/j.epsl.2008.07.016

Li, Y., & Audétat, A. (2012). Partitioning of V, Mn, Co, Ni, Cu, Zn, As, Mo, Ag, Sn, Sb, W, Au, Pb, and Bi between sulfide phases and hydrous basanite melts at upper mantle conditions. *Earth and Planetary Science Letters*, *355–356*, 327–340. https://doi.org/10.1016/j.epsl.2012.08.008

Liang, Y.-H., Halliday, A. N., Siebert, C., Fitton, J. G., Burton, K. W., Wang, K.-L., & Harvey, J. (2017). Molybdenum isotope fractionation in the mantle. *Geochimica et Cosmochimica Acta*, *199*, 91–111. https://doi.org/10.1016/j.gca.2016.11.023

Liu, C.-Z., Wu, F.-Y., Sun, J., Chu, Z.-Y., & Yu, X.-H. (2013). Petrology, geochemistry and Re-Os isotopes of peridotites xenoliths from Maguan, Yunnan Province: Implications for the Cenozoic mantle replacement in southwestern China. *Lithos*, *168–169*, 1–14. https://doi.org/10.1016/j.lithos.2013.01.011

Liu, S.-A., Wang, Z.-Z., Yang, C., Li, S.-G., & Ke, S. (2020). Mg and Zn isotope evidence for two types of mantle metasomatism and deep recycling of magnesium carbonates. *Journal of Geophysical Research: Solid Earth*, *125*(11), e2020JB020684. https://doi.org/10.1029/2020JB020684

Ma, L., Xu, Y.-G., Li, J., Chen, L.-H., Liu, J.-Q., Li, H.-Y., et al. (2022). Molybdenum isotopic constraints on the origin of EM1-type continental intraplate basalts. *Geochimica et Cosmochimica Acta*, *317*, 255–268. https://doi.org/10.1016/j.gca.2021.11.013

McCoy-West, A. J., Chowdhury, P., Burton, K. W., Sossi, P., Nowell, G. M., Fitton, J. G., et al. (2019). Extensive crustal extraction in Earth's early history inferred from molybdenum isotopes. *Nature Geoscience*, *12*(11), 946–951. https://doi.org/10.1038/s41561-019-0451-2

McDonough, W., & Sun, S. s. (1995). The composition of the Earth. *Chemical Geology*, *120*(3–4), 223–253. https://doi.org/10.1016/0009-2541(94)00140-4

Neubert, N., Nägler, T. F., & Böttcher, M. E. (2008). Sulfidity controls molybdenum isotope fractionation into euxinic sediments: Evidence from the modern Black Sea. *Geology*, *36*(10), 775–778. https://doi.org/10.1130/G24959A.1

Newsom, H. E., White, W. M., Jochum, K. P., & Hofmann, A. W. (1986). Siderophile and chalcophile element abundances in oceanic basalts, Pb isotope evolution and growth of the Earth's core. *Earth and Planetary Science Letters*, *80*(3–4), 299–313. https://doi.org/10.1016/0012-821X(86)90112-3

Nie, X., Feng, Q., Qian, X., & Wang, Y. (2015). Magmatic record of Prototethyan evolution in SW Yunnan, China: Geochemical, zircon U–Pb geochronological and Lu–Hf isotopic evidence from the Huimin metavolcanic rocks in the southern Lancangjiang zone. *Gondwana Research*, *8*(2), 757–768. https://doi.org/10.1016/j.gr.2014.05.011

Peacock, S. M. (1990). Fluid processes in subduction zones. *Science*, *248*(4953), 329–337. https://doi.org/10.1126/science.248.4953.32

Plank, T. (2014). The chemical composition of subducting sediments. In H. D. Holland & K. K. Turekian (Eds.), *Treatise on geochemistry* (2nd ed., pp. 607–629). Elsevier. https://doi.org/10.1016/B978-0-08-095975-7.00319-3

Reinhard, A. A., Jackson, M. G., Blusztajn, J., Koppers, A. A. P., Simms, A. R., & Konter, J. G. (2019). "Petit Spot" rejuvenated volcanism superimposed on plume-derived Samoan shield volcanoes: Evidence from a 645-m drill core from Tutuila Island, American Samoa. *Geochemistry, Geophysics, Geosystems*, *20*(3), 1485–1507. https://doi.org/10.1029/2018GC007985

Rojas-Kolomiets, E., Jensen, O., Bizimis, M., Yogodzinski, G., & Ackerman, L. (2023). Serpentinite fluids and slab-melting in the Aleutian arc: Evidence from molybdenum isotopes and boron systematics. *Earth and Planetary Science Letters*, *603*, 117970. https://doi.org/10.1016/j.epsl.2022.117970

Rollinson, H. (1993). *Using geochemical data: Evaluation, presentation, interpretation* (1st ed.). Routledge. https://doi.org/10.4324/9781315845548

Rudnick, R. L., Barth, M., Horn, I., & McDonough, W. F. (2000). Rutile-bearing refractory eclogites: Missing link between continents and depleted mantle. *Science*, *287*(5451), 278–281. https://doi.org/10.1126/science.287.5451.278

Rudnick, R. L., & Gao, S. (2014). Composition of the continental crust. In H. D. Holland & K. K. Turekian (Eds.), *Treatise on geochemistry* (2nd ed., pp. 1–51). Elsevier. https://doi.org/10.1016/B978-0-08-095975-7.00301-6

Spandler, C., & Pirard, C. (2013). Element recycling from subducting slabs to arc crust: A review. *Lithos*, *170–171*, 208–223. https://doi.org/10.1016/j.lithos.2013.02.016

Spera, F. J. (1984). Carbon dioxide in petrogenesis III: Role of volatiles in the ascent of alkaline magma with special reference to xenolith-bearing mafic lavas. *Contributions to Mineralogy and Petrology*, *88*(3), 217–232. https://doi.org/10.1007/BF00380167

Sun, C., Zhao, Z., Mo, X., Zhu, D., Dong, G., Zhou, S., et al. (2007). Geochemistry and petrogenesis of Miocene Sailipu ultrapotassic rocks in western Lhasa Block, Tibetan Plateau (in Chinese with English abstract). *Acta Petrologica Sinica*, *11*, 2715–2726. https://doi.org/10.3969/j.issn.1000-0569.2007.11.004

Sun, S. S., & McDonough, W. F. (1989). Chemical and isotopic systematics of oceanic basalts: Implications for mantle composition and processes. *Geological Society of London Special Publications*, *42*(1), 313–345. https://doi.org/10.1144/GSL.SP.1989.042.01.19

Syracuse, E. M., van Keken, P. E., & Abers, G. A. (2010). The global range of subduction zone thermal models. *Physics of the Earth and Planetary Interiors*, *183*, 73–90. https://doi.org/10.1016/j.pepi.2010.02.004

Tapponnier, P., Peltzer, G., Dain, A., Armijo, R., & Cobbold, P. (1982). Propagating extrusion tectonics in Asia: New insights from simple experiments with plasticine. *Geology*, *10*(12), 611–616. https://doi.org/10.1130/0091-7613(1982)10<611:PETIAN>2.0.CO;2

Teng, F.-Z., Dauphas, N., & Watkins, J. M. (2017). Non-traditional stable isotopes: Retrospective and prospective. *Reviews in Mineralogy and Geochemistry*, *82*(1), 1–26. https://doi.org/10.2138/rmg.2017.82.1

Tian, H.-C., Yang, W., Li, S.-G., Ke, S., & Chu, Z.-Y. (2016). Origin of low δ^{26}Mg basalts with EM-I component: Evidence for interaction between enriched lithosphere and carbonated asthenosphere. *Geochimica et Cosmochimica Acta*, *188*, 93–105. https://doi.org/10.1016/j.gca.2016.05.021

van Hinsbergen, D. J. J. (2022). Indian plate paleogeography, subduction and horizontal underthrusting below Tibet: Paradoxes, controversies and opportunities. *National Science Review*, *9*(8), nwac074. https://doi.org/10.1093/nsr/nwac074

van Hinsbergen, D. J. J., Spakman, W., de Boorder, H., van Dongen, M., Jowitt, S. M., & Mason, P. R. D. (2020). Arc-type magmatism due to continental-edge plowing through ancient subduction-enriched mantle. *Geophysical Research Letters*, *47*(9), e2020GL087484. https://doi.org/10.1029/2020GL087484

van Keken, P. E., Hacker, B. R., Syracuse, E. M., & Abers, G. A. (2011). Subduction factory: 4. Depth-dependent flux of H_2O from subducting slabs worldwide. *Journal of Geophysical Research*, *116*, B01401. https://doi.org/10.1029/2010JB007922

Voegelin, A. R., Nägler, T. F., Pettke, T., Neubert, N., Steinmann, M., Pourret, O., & Villa, I. M. (2012). The impact of igneous bedrock weathering on the Mo isotopic composition of stream waters: Natural samples and laboratory experiments. *Geochimica et Cosmochimica Acta*, *86*, 150–165. https://doi.org/10.1016/j.gca.2012.02.029

Voegelin, A. R., Pettke, T., Greber, N. D., von Niederhäusern, B., & Nägler, T. F. (2014). Magma differentiation fractionates Mo isotope ratios: Evidence from the Kos Plateau Tuff (Aegean Arc). *Lithos*, *190–191*, 440–448. https://doi.org/10.1016/j.lithos.2013.12.016

Wada, I., Behn, M. D., & Shaw, A. M. (2012). Effects of heterogeneous hydration in the incoming plate, slab rehydration, and mantle wedge hydration on slab-derived H_2O flux in subduction zones. *Earth and Planetary Science Letters*, *353–354*, 60–71. https://doi.org/10.1016/j.epsl.2012.07.025

Wagner, L. J., Kleinhanns, I. C., Varas-Reus, M. I., Rosca, C., König, S., Bach, W., & Schoenberg, R. (2023). Light stable Cr isotope compositions of mid-ocean ridge basalts: Implications for mantle source composition. *Geochimica et Cosmochimica Acta*, *353*, 76–91. https://doi.org/10.1016/j.gca.2023.04.028

Wang, J., Tang, G.-J., Tappe, S., Li, J., Zou, Z., Wang, Q., et al. (2024). Tracing subducted carbonates in Earth's mantle using zinc and molybdenum isotopes. *Geophysical Research Letters*, *51*(4), e2023GL105208. https://doi.org/10.1029/2023GL105208

Wang, J., Wang, Q., Xu, C.-B., Dan, W., Xiao, Z., Shu, C., & Wei, G. (2022). Cenozoic delamination of the southwestern Yangtze craton owing to densification during subduction and collision. *Geology*, *50*(8), 912–917. https://doi.org/10.1130/G49732.1

Wang, J.-H., Yin, A., Harrison, T. M., Grove, M., Zhang, Y.-Q., & Xie, G.-H. (2001). A tectonic model for Cenozoic igneous activities in the eastern Indo–Asian collision zone. *Earth and Planetary Science Letters*, *188*(1–2), 123–133. https://doi.org/10.1016/S0012-821X(01)00315-6

Wang, X., Metcalfe, I., Jian, P., He, L., & Wang, C. (2000). The Jinshajiang–Ailaoshan suture zone, China: Tectonostratigraphy, age and evolution. *Journal of Asian Earth Sciences*, *18*(6), 675–690. https://doi.org/10.1016/S1367-9120(00)00039-0

Wang, Z., & Becker, H. (2018). Molybdenum partitioning behavior and content in the depleted mantle: Insights from Balmuccia and Baldissero mantle tectonites (Ivrea Zone, Italian Alps). *Chemical Geology*, *499*, 138–150. https://doi.org/10.1016/j.chemgeo.2018.09.023

Wang, Z.-Z., & Liu, S.-A. (2021). Evolution of intraplate alkaline to tholeiitic basalts via interaction between carbonated melts and lithospheric mantle. *Journal of Petrology*, *62*(4), egab025. https://doi.org/10.1093/petrology/egab025

Wang, Z.-Z., Liu, S.-A., Chen, L.-H., Li, S.-G., & Zeng, G. (2018). Compositional transition in natural alkaline lavas through silica-undersaturated melts–lithosphere interaction. *Geology*, *46*(9), 771–774. https://doi.org/10.1130/G45145.1

Weaver, B. L. (1991). The origin of ocean island basalt end-member compositions: Trace element and isotopic constraints. *Earth and Planetary Science Letters*, *104*(2–4), 381–397. https://doi.org/10.1016/0012-821X(91)90217-6

Willbold, M., & Elliott, T. (2017). Molybdenum isotope variations in magmatic rocks. *Chemical Geology*, *449*, 253–268. https://doi.org/10.1016/j.chemgeo.2016.12.011

Willbold, M., & Elliott, T. (2023). Molybdenum isotope evidence for subduction-modified, recycled mafic oceanic crusts in the mantle sources of ocean island basalts from La Palma and Hawaii. *Earth and Planetary Science Letters*, *621*, 118399. https://doi.org/10.1016/j.epsl.2023.118399

Willbold, M., Hibbert, K., Lai, Y.-J., Freymuth, H., Hin, R. C., Coath, C., et al. (2016). High-precision mass-dependent molybdenum isotope variations in magmatic rocks determined by double-spike MC-ICP-MS. *Geostandards and Geoanalytical Research*, *40*(3), 389–403. https://doi.org/10.1111/j.1751-908X.2015.00388.x

Wille, M., Nebel, O., Pettke, T., Vroon, P. Z., König, S., & Schoenberg, R. (2018). Molybdenum isotope variations in calc-alkaline lavas from the Banda arc, Indonesia: Assessing the effect of crystal fractionation in creating isotopically heavy continental crust. *Chemical Geology*, *485*, 1–13. https://doi.org/10.1016/j.chemgeo.2018.02.037

Xia, P., & Xu, Y.-G. (2006). Mantle-derived xenoliths in Maguan Cenozoic potassic basalt, Southeast Yunnan and its bearing on lithospheric composition and dynamics (in Chinese with English abstract). *Geochimica*, *35*, 27–40.

Xie, Q., Zhang, Z., Foley, S. F., Chen, C., Cheng, Z., Wang, Y., et al. (2023). Transition from tholeiitic to alkali basalts via interaction between decarbonated eclogite-derived melts and peridotites. *Chemical Geology*, *621*, 121354. https://doi.org/10.1016/j.chemgeo.2023.121354

Xu, D., Qi, Y., & Wang, Q. (2024). Indentifying materials using Mo isotopes in intraplate alkali basalts from southeastern margin of Tibetan Plateau [Dataset]. *Figshare*. https://doi.org/10.6084/m9.figshare.25965397

Xu, L., Lehmann, B., Mao, J., Nägler, T. F., Neubert, N., Böttcher, M. E., & Escher, P. (2012). Mo isotope and trace element patterns of Lower Cambrian black shales in South China: Multi-proxy constraints on the paleoenvironment. *Chemical Geology*, *318–319*, 45–59. https://doi.org/10.1016/j.chemgeo.2012.05.016

Xu, M., Huang, H., Huang, Z., Wang, P., Wang, L., Xu, M., et al. (2018). Insight into the subducted Indian slab and origin of the Tengchong volcano in SE Tibet from receiver function analysis. *Earth and Planetary Science Letters*, *482*, 567–579. https://doi.org/10.1016/j.epsl.2017.11.048

Yin, A., & Taylor, M. H. (2011). Mechanics of V-shaped conjugate strike-slip faults and the corresponding continuum mode of continental deformation. *Geological Society of America Bulletin*, *123*(9–10), 1798–1821. https://doi.org/10.1130/B30159.1

Yu, Y., Huang, X.-L., Chung, S.-L., Li, J., Lai, Y.-M., Setiawan, I., & Sun, M. (2022). Molybdenum isotopic constraint from Java on slab inputs to subduction zone magmatism. *Geochimica et Cosmochimica Acta*, *332*, 1–18. https://doi.org/10.1016/j.gca.2022.06.009

Zhang, H.-F., Sun, M., Zhou, X.-H., Zhou, M.-F., Fan, W.-M., & Zheng, J.-P. (2003). Secular evolution of the lithosphere beneath the eastern North China Craton: Evidence from Mesozoic basalts and high-Mg andesites. *Geochimica et Cosmochimica Acta*, *67*(22), 4373–4387. https://doi.org/10.1016/S0016-7037(03)00377-6

Zhang, L., Li, J., Zang, Y., Peng, B.-Y., Wang, Z.-B., & Ren, Z.-Y. (2024). Molybdenum isotopic fractionation in the Panzhihua mafic layered intrusion in the Emeishan large igneous province, southwest China. *American Mineralogist*, *109*(3), 628–632. https://doi.org/10.2138/am-2023-9154

Zhang, Y., Yuan, C., Sun, M., Chen, M., Hong, L., Li, J., et al. (2019). Recycled oceanic crusts in the form of pyroxenites contributing to the Cenozoic continental basalts in central Asia: New perspectives from olivine chemistry and whole-rock B–Mo isotopes. *Contributions to Mineralogy and Petrology*, *174*(10), 83. https://doi.org/10.1007/s00410-019-1620-4

Zhang, Y., Yuan, C., Sun, M., Li, J., Long, X., Jiang, Y., & Huang, Z. (2020). Molybdenum and boron isotopic evidence for carbon-recycling via carbonate dissolution in subduction zones. *Geochimica et Cosmochimica Acta*, *278*, 340–352. https://doi.org/10.1016/j.gca.2019.12.013

Zhao, P.-P., Li, J., Zhang, L., Wang, Z.-B., Kong, D.-X., Ma, J.-L., et al. (2016). Molybdenum mass fractions and isotopic compositions of international geological reference materials. *Geostandards and Geoanalytical Research*, *40*(2), 217–226. https://doi.org/10.1111/j.1751-908X.2015.00373.x

Zhu, R.-X., Xu, Y.-G., Zhu, G., Zhang, H.-F., Xia, Q.-K., & Zheng, T.-Y. (2012). Destruction of the North China Craton. *Science China Earth Sciences*, *42*(8), 1135–1159. https://doi.org/10.1007/s11430-012-4516-y

Zindler, A., & Hart, S. R. (1986). Chemical geodynamics. *Annual Review of Earth and Planetary Sciences*, *14*(1), 493–571. https://doi.org/10.1146/annurev.ea.14.050186.002425

Zou, Z., Wang, Z., Foley, S., Xu, R., Geng, X., Liu, Y.-N., et al. (2022). Origin of low-MgO primitive intraplate alkaline basalts from partial melting of carbonate-bearing eclogite sources. *Geochimica et Cosmochimica Acta*, *324*, 240–261. https://doi.org/10.1016/j.gca.2022.02.022

References From the Supporting Information

Dai, F.-Q., Zhao, Z.-F., Dai, L.-Q., & Zheng, Y.-F. (2016). Slab–mantle interaction in the petrogenesis of andesitic magmas: Geochemical evidence from postcollisional intermediate volcanic rocks in the Dabie Orogen, China. *Journal of Petrology*, *57*(6), 1109–1134. https://doi.org/10.1093/petrology/egw034

Koppers, A. A. P. (2002). ArArCALC—Software for $^{40}Ar/^{39}Ar$ age calculations. *Computers & Geosciences*, *28*(5), 605–619. https://doi.org/10.1016/S0098-3004(01)00095-4

Li, J., Liang, X.-R., Zhong, L.-F., Wang, X.-C., Ren, Z.-Y., Sun, S.-L., et al. (2014). Measurement of the isotopic composition of molybdenum in geological samples by MC-ICP-MS using a novel chromatographic extraction technique. *Geostandards and Geoanalytical Research*, *38*(3), 345–354. https://doi.org/10.1111/j.1751-908X.2013.00279.x

Li, X.-H., Zhou, H., Chung, S.-L., Lo, C.-H., Wei, G., Liu, Y., & Lee, C.-Y. (2002). Geochemical and Sr-Nd isotopic characteristics of late Paleogene ultrapotassic magmatism in southeastern Tibet. *International Geological Review*, *44*(6), 559–574. https://doi.org/10.2747/0020-6814.44.6.559

Weis, D., Kieffer, B., Maerschalk, C., Pretorius, W., & Barling, J. (2005). High-precision Pb-Sr-Nd-Hf isotopic characterization of USGS BHVO-1 and BHVO-2 reference materials. *Geochemistry, Geophysics, Geosystems*, *6*(2). https://doi.org/10.1029/2004GC000852

Xing, C.-M., Wang, C. Y., Charlier, B., & Namur, O. (2022). Ubiquitous dendritic olivine constructs initial crystal framework of mafic magma chamber. *Earth and Planetary Science Letters*, *594*, 117710. https://doi.org/10.1016/j.epsl.2022.117710

Zhang, W.-F., Li, J.-J., Zheng, D.-W., Sun, S.-H., Guo, Y.-F., Zhang, J., et al. (2023). Sample neutron irradiation with the Min Jiang Testing Reactor (MJTR) implications for high-precision $^{40}Ar/^{39}Ar$ dating. *Journal of Analytical Atomic Spectrometry*, *38*(8), 1540–1548. https://doi.org/10.1039/D3JA00048F